Hail Risk and Cropland Exposure Changes in the United States

LOGAN R. BUNDY,[a] WALKER S. ASHLEY,[a] ALEX M. HABERLIE,[a] STEPHEN M. STRADER,[b] VITTORIO A. GENSINI,[a] ALLISON C. MICHAELIS,[c] MARGO S. ANDREWS,[a] AND EVELYNN MANTIA[a]

[a] *Department of Earth, Atmosphere, and Environment, Northern Illinois University, DeKalb, Illinois*
[b] *Department of Geography and the Environment, Villanova University, Villanova, Pennsylvania*
[c] *Department of Marine, Earth, and Atmospheric Science, North Carolina State University, Raleigh, North Carolina*

(Manuscript received 15 October 2025, in final form 13 July 2026, accepted 24 July 2026)

ABSTRACT: The U.S. agricultural landscape is ever-evolving, with uncertainty in future losses driven by cropland exposure interacting with a changing weather and climate risk landscape. Among these weather hazards is hail—currently the third-costliest peril affecting crop production in the United States. This research employs a combination of historical and future projection cropland layers, observed severe hail reports, crop-hail insurance data, and output from convection-permitting climate simulations to demonstrate the interrelationship between changing cropland exposure and hail risk during the twenty-first century. Impacts of weather hazards on buildings, infrastructure, and other societal assets are driven by an expanding exposure footprint, and agricultural systems may follow similar trends in some U.S. regions. Results from a Monte Carlo simulation reveal that, while Midwest cropland is most exposed to hail, the Great Plains contain the highest vulnerability based on the collocation of an extensive hail footprint during the summer growing season and the expansion of cropland. Despite projected decreases in severe hail days in the Great Plains, the increase in regional cropland exposure illustrates the "expanding bull's-eye effect" concept within the context of agriculture, highlighting that disaster potential (i.e., major crop yield loss) is not solely determined by the total area of cropland; rather, it is how croplands are distributed across the landscape that defines how risk and vulnerability are realized in a major crop loss scenario. Results from this research may inform data-driven decision-making efforts and risk communication across the agricultural community, including stakeholders in crop insurance, sustainability, and other pursuits in regional climatology.

SIGNIFICANCE STATEMENT: The purpose of this study is to understand how the crop-hail risk landscape may change through the twenty-first century. The agricultural landscape continuously evolves, with increasing uncertainty in future losses driven by cropland exposure interacting with a changing weather and climate risk landscape. Results indicate regional variation, as the Great Plains face the greatest exposure-driven risk, reflecting the "expanding bull's-eye effect" in an agricultural context. Meanwhile, the Midwest and South may undergo hazard-driven loss increases despite negligible change in cropland extent. These findings highlight the need for proactive, regionally tailored adaptation strategies, offering a novel basis for understanding future crop-hail risk.

KEYWORDS: Hail; Climate models; Agriculture; Crop growth; Decision support; Land use

1. Introduction and background

Since the mid-nineteenth century, agricultural land cover across the United States has expanded nearly fivefold (Yu and Lu 2018), with substantial growth in areas with erosive soils, poor drainage, nutrient deficiencies, and climatic stress (Lark et al. 2015, 2020). In recent decades, much of the expansion has been focused across the Great Plains (Lark et al. 2015, 2020), driven by land conversion due to changes in agricultural practices, including grassland-to-cropland conversion, crop rotation, and the expansion of row crop production (Ramankutty and Foley 1999a,b; Lark et al. 2015; Wimberly et al. 2017; Lark et al. 2019, 2020). Today's cropland expansion is directly associated with heightened crop demand due to global population growth, increases in biofuel production, and changes in human dietary trends (Cassidy et al. 2013), which encourages the conversion of remaining natural landscapes to agricultural land (West et al. 2010; Johnson et al. 2014). Agriculture is increasingly shaped not only by biophysical stressors but also by societal and economic vulnerabilities. Therefore, expanding cropland into hazard-prone regions amplifies exposure to weather extremes for producers, insurers, and rural communities (Bolster et al. 2023).

Hail risk in the United States has been widely studied from both climatological (Cintineo et al. 2012; Tang et al. 2019) and agricultural perspectives (Changnon et al. 2009; Reyes and Elias 2019; Bundy et al. 2022). Hail represents a particularly acute peril, with impacts that extend beyond physical crop damage. Severe hail can bruise grain and fruit, damage stems, cause leaf defoliation, reduce kernel or pod quality, and introduce disease pathways, thereby affecting crop yields (Vorst 1993; Changnon et al. 2009; Klein and Shapiro 2011; Battaglia et al. 2019; Lindsey et al. 2024; Lisboa et al. 2024). These direct crop impacts can cascade through agricultural systems by decreasing marketability, altering commodity

Supplemental information related to this paper is available at the Journals Online website: https://doi.org/10.1175/WCAS-D-25-0160.s1.

Corresponding author: Logan R. Bundy, lbundy@niu.edu

DOI: 10.1175/WCAS-D-25-0160.1

© 2026 American Meteorological Society. This published article is licensed under the terms of the default AMS reuse license. For information regarding reuse of this content and general copyright information, consult the AMS Copyright Policy (www.ametsoc.org/PUBSReuseLicenses).

Authenticated lbundy@niu.edu | Downloaded 09/03/26 01:39 PM UTC

pricing, and creating financial strain on crop producers and rural economies where agriculture represents a dominant sector (Bolster et al. 2023). Financially, hail losses are absorbed both privately and publicly, with insured crop losses due to hail summing to over 800 million USD annually [Changnon et al. 2009; adjusted to 2023 consumer price index (CPI)]. Hail poses a unique challenge for agricultural systems because the occurrence, location, and severity of hail are difficult to forecast with enough lead time to implement effective mitigation measures across farming operations, leaving crops vulnerable to rapid and extensive loss (Changnon et al. 2001). The extent of crop damage depends not only on hailstone size, hailstone quantity, and associated winds from a severe thunderstorm (Changnon 1999; Changnon et al. 2009) but also on crop type, hybrid, and phenological stage (Lindsey et al. 2024). Therefore, the sudden onset of hail, coupled with increasing spatial overlap of cropland and hail-prone regions, underscores the societal importance of anticipating how these risks evolve.

Escalating losses and disasters are a function of climatological risk—the probability of a weather- or climate-related hazard occurring in space and time, the exposure of goods and people to a specific hazard, and the vulnerability of exposed people, infrastructure, and the environment (IPCC 2014). Moreover, previous research has argued that increasing human exposure contributes more to resulting property damage totals than increases in the frequency and severity of natural hazards (Changnon et al. 1997; Janković and Schultz 2017; Rosencrants and Ashley 2015; Strader et al. 2024). The "expanding bull's-eye effect" concept, developed to describe how increasing human exposure in the path of a hazard increases the severity of loss (Ashley et al. 2014; Rosencrants and Ashley 2015; Ashley and Strader 2016; Freeman and Ashley 2017; Strader 2018; Strader et al. 2015a,b, 2017a,b, 2018, 2024), provides a useful framework for understanding hail risk and agriculture. This concept has been applied indirectly to agriculture (e.g., Lobell et al. 2014; Li et al. 2019; Bundy et al. 2022, 2024, 2026), but these indirect applications of the expanding bull's-eye effect concept fall short in quantifying the exposure factor—the underlying cropland surface—as a potential driver of agricultural loss.

This study investigates the question: How may the crop-hail risk landscape change? To thoroughly answer this question, the objectives of this research are to 1) quantify future-projected cropland changes, 2) spatially demonstrate historical and future cropland exposure risk to hail for key U.S. agricultural regions, and 3) further the understanding of hail in future climates juxtaposed with future cropland exposure. This research is novel in that it is the first to directly use the expanding bull's-eye effect concept to understand the impact of cropland exposure when assessing hail risk. Additionally, this study is the first to examine future cropland coverage scenarios combined with future-projected severe hail days during the mid- and end-of-twenty-first century. The results provide decision-relevant insights for crop producers, insurers, and policymakers, as understanding how projected cropland changes intersect with future hail risk is critical for guiding adaptation strategies, structuring insurance programs, and sustaining agricultural resilience against extreme weather perils.

2. Data and methods

a. Data background and collection

1) USGS LAND-COVER DATA

Three U.S. Geological Survey (USGS) land-cover datasets were used: modeled historical land cover (1938–92; Sohl et al. 2018a), historical baseline land cover (1992–2005; Sohl et al. 2018b), and land-cover projections (2006–2100; Sohl et al. 2018b). All data provide a cropland class at 250-m resolution for the conterminous United States (CONUS). The Forecasting Scenarios of Land-Use Change (FORE-SCE) model was employed to generate the modeled historical land-cover dataset, which uses USDA Land Cover Trends data, USDA Census of Agriculture data, and a series of theoretical, statistical, and deterministic modeling techniques to estimate land cover (Sohl et al. 2007, 2012, 2014). Like the modeled historical land-use/land-cover (LULC) data, projected LULC data were developed using the FORE-SCE, corresponding to the four major scenario storylines from the Intergovernmental Panel on Climate Change (IPCC) Special Report on Emissions Scenarios (SRES): A1B, A2, B1, and B2. The four major scenarios focused on socioeconomic impacts on anthropogenic land use, with distinctly different directions for future developments (Nakicenovic et al. 2000):

- A1B: Scenario promotes rapid economic growth, with global population peaking during the midcentury, but a decline in population during the remainder of the twenty-first century. More efficient technologies are introduced along with a balance between fossil-intensive and nonfossil energy sources. The underlying themes consist of convergence among regions, capacity building, increased cultural and social interactions, and a reduction in regional differences in per capita income.
- A2: The underlying theme of this scenario is self-reliance and the preservation of local identities in a very heterogeneous world. Fertility patterns converge slowly across regions, resulting in a continuously increasing population. Also, economic development is primarily regionally oriented, and per capita growth and technological changes are slower than in other scenarios.
- B1: Scenario demonstrates a convergent world with a steady global population that peaks in midcentury but declines thereafter. There are rapid changes in economic structures toward a service and information economy. A reduction in material intensity is introduced along with the use of clean and efficient technologies. The emphasis is on global sustainability solutions but without additional climate initiatives.
- B2: The emphasis is on local solutions to economic, social, and environmental sustainability, alongside a continuously increasing global population, but at a rate lower than the A2 scenario. There are intermediate levels of economic development with less rapid but more diverse technological changes than in the B1 and A1B scenarios. This scenario is oriented toward environmental protection and social equity at local and regional levels.

SRES scenarios differ in two primary dimensions: economic development (A1B and A2) or environmental concern (B1 and

Authenticated lbundy@niu.edu | Downloaded 09/03/26 01:39 PM UTC

B2) and either global (A1B and B1) or regional development patterns (A2 and B2). Therefore, each category can be referred to as global economic (A1B), local economic (A2), global environmental (B1), and local environmental (B2) scenarios. Historical cropland layers were collected for 1950 and 2005 and projections for 2055 and 2100, aligning with hail simulation periods (described below).

2) USDA NASS DATA

County-level yield, planted, and harvested acreage data from the USDA National Agricultural Statistics Service (NASS) QuickStats database (1990–2020) were used to provide context for regional crop selections. Corn, cotton, sorghum, soybeans, and wheat were selected due to their dominance in U.S. production (~90% of national production in 2023; NASS 2024) and represent recent Great Plains cropland expansion (Lark et al. 2015). These data were not directly integrated into the modeling but informed discussion of cropland exposure and phenological vulnerability.

3) USDA RMA INSURANCE DATA

Monthly, county-level crop insurance data from the USDA Risk Management Agency (RMA) Summary of Business and Cause of Loss database (1990–2020) were analyzed for May–October. Corn, cotton, sorghum, soybeans, and wheat were used from this dataset to remain consistent with the NASS yield, planting, and harvesting data. Due to interannual changes in commodity prices, inflation, insurance coverage, RMA program policies, and socioeconomic conditions, crop indemnities are not comparable across growing seasons without standardizing the data (Changnon and Hewings 2001; Barthel and Neumayer 2012). Payment indemnity and liability data were inflation-adjusted to 2023 USD and detrended to remove long-term trends, thereby improving the isolation of weather-related impacts on agriculture. Additionally, the loss cost (indemnity/liability × 100) was calculated (Changnon 1972), which is a normalized ratio that accounts for the value of products (Reyes and Elias 2019) and has been extensively used in agricultural research (e.g., Coble and Barnett 2013; Reyes and Elias 2019; Perry et al. 2020; Reyes et al. 2020).

4) NOAA SPC SVRGIS DATA

Historical hail risk, or the hail climatology, was quantified using the spatial and temporal attributes of severe hail reports [Storm Prediction Center (SPC) 2024]. A severe hail day was defined as at least one severe hail report (≥1.0 in.; 2.54-cm diameter) day^{-1} within an 80-km grid, following SPC's severe storm verification process (Gensini et al. 2020). Gridded hail days within the growing season were then aggregated to the county level to align with crop-hail RMA insurance data. While hailstones that are <1.0 in. (<2.54 cm) in diameter can be damaging to crops (Changnon 1999; Changnon et al. 2001), severe hail days were used as opposed to all hail days because of the insufficient record of smaller hail sizes, which holds true even across radar-derived hail datasets (e.g., Cecil and Blankenship 2012; Murillo et al. 2021) and high-resolution, regional climate simulations (Gensini et al. 2024). Hail observations also present challenges, as the Severe Weather GIS (SVRGIS) dataset reflects known reporting biases (Allen and Tippett 2015). By focusing on severe hail days aggregated to an 80-km grid, the analysis minimizes these nonmeteorological uncertainties and emphasizes events most likely to generate extensive agricultural loss, making the results conservative but highly relevant for decision-making.

5) WRF-BCC REGIONAL CLIMATE MODEL DATA

Dynamically downscaled convection-permitting Weather Research and Forecasting (WRF) Model simulations, configured by the bias-corrected Community Earth System Model (WRF-BCC; Gensini et al. 2023), were used to estimate the severe hail climatology for a historical period (HIST; 1990–2005), midcentury period (MID; 2040–55), and end-of-century period (END; 2085–2100). Here, dynamical downscaling involves using coarse-resolution climate model output to provide initial and lateral boundary conditions for convection-permitting simulations. These higher-resolution simulations explicitly capture meso-γ processes associated with hailstorms (Gensini et al. 2024), and the use of dynamical downscaling has been widely applied to evaluate both historical and future changes in convective storm populations (Trapp et al. 2011; Robinson et al. 2013; Gensini and Mote 2014, 2015; Hoogewind et al. 2017; Liu et al. 2017; Prein et al. 2017; Trapp et al. 2019; Haberlie et al. 2022; Ashley et al. 2023). A horizontal grid spacing of 3.75 km permitted the simulations to explicitly (without a convective parameterization scheme) simulate the deep, moist convection responsible for hail production (Weisman et al. 1997; Kendon et al. 2021) and permits the formation of individual hailstorms (Ashley et al. 2023; Gensini et al. 2024). Hail size and frequency from WRF-BCC are directly represented through an inline spectral bulk microphysics scheme, allowing for physically consistent estimation of hail characteristics across historical and future climates (Gensini et al. 2024). Importantly, this approach realistically captures the spatial and seasonal climatology of severe convective environments across the United States (Ashley et al. 2023; Haberlie et al. 2024; Gensini et al. 2024).

WRF-BCC simulations were conducted using representative concentration pathways (RCPs) 4.5 and 8.5, consistent with forcing scenarios used in the IPCC Fifth Assessment Report (IPCC 2014). RCP4.5 represents an intermediate stabilization pathway in which radiative forcing levels off by 2100 without overshoot (Thomson et al. 2011), whereas RCP8.5 reflects a higher-emission pathway characterized by substantially greater radiative forcing (Riahi et al. 2011). Although RCP8.5 is considered improbable, it is still widely used in climate impact studies to represent an upper-bound scenario and to facilitate comparison with the extensive CMIP5-based literature (Hausfather and Peters 2020; Schwalm et al. 2020). Herein, the five sets of simulations, each spanning 15 hydrologic years (1 October–30 September), will be referred to as HIST, MID4.5, MID8.5, END4.5, and END8.5, consistent with prior literature using WRF-BCC climate simulations (e.g., Ashley et al. 2023; Zeeb et al. 2024; Gensini et al. 2024; Haberlie et al. 2024; Stinnett et al. 2024; Kaminski et al. 2025;

Authenticated lbundy@niu.edu | Downloaded 09/03/26 01:39 PM UTC

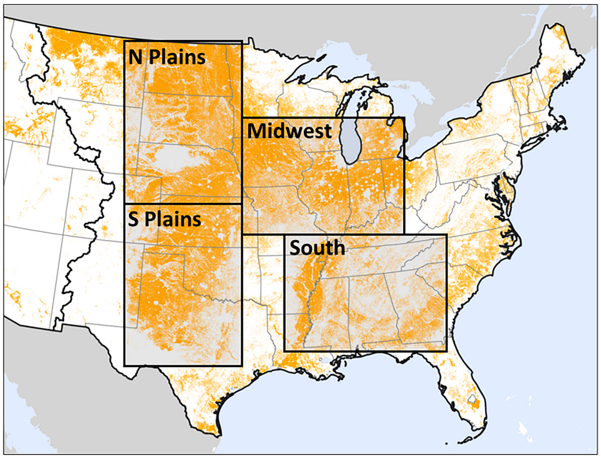

FIG. 1. Study domain with four equal-area study regions east of the U.S. Continental Divide. Cropland presence (cropland vs noncropland) from the A2 2100 scenario is displayed in orange at 250-m resolution.

Wallace et al. 2025). Further details on WRF-BCC model configuration are provided in Gensini et al. (2023).

Analyses herein used the daily maximum value of the hail_maxk1 variable—the maximum diameter of graupel/hail diagnosed in the Thompson microphysics scheme (Thompson et al. 2008) at the model level closest to the surface. WRF-BCC analyses will focus on hail ≥ 1.25 in. (3.15 cm) in diameter. The 1.25-in. threshold is consistent with prior literature's selection for severe hail following an analysis of WRF-BCC hail_maxk1 compared to the SVRGIS and GridRad datasets (Gensini et al. 2024). Here, a severe hail day is defined as at least one instance per day of the hail_maxk1 variable meeting or exceeding the 1.25-in. threshold at a grid point (Allen and Tippett 2015; Trapp et al. 2019). A comparison of WRF-BCC and SVRGIS growing-season severe hail days on similar, roughly 80-km grids reveals that WRF-BCC simulations successfully reproduce the number of observed severe hail days, but they do exhibit a westward spatial bias in the location of maximum severe hail days as well as a low bias east of the Mississippi River (Fig. 1 in the online supplemental material).

b. *Methods*

1) CLIMATOLOGY

For crop production or yield loss to occur due to hail, an explicit hail risk must be present at the given location. Thus, to thoroughly assess the expanding bull's-eye effect—where increasing exposure (e.g., cropland expansion) amplifies impacts through greater overlap with hazardous events—within an agricultural context, a general crop-hail climatology (1990–2020) needs to be established to understand baseline risk. Therefore, within agriculture, the expanding bull's-eye effect is only relevant in regions where cropland exposure spatially overlaps with an existing climatological hazard risk. For the crop-hail climatology, SVRGIS severe hail data were used to calculate the mean number of severe hail days in each boreal summer growing season (May–October) at the county level over the 1990–2020 period. The number of severe hail days for each growing season was also compared with the 1990–2020 mean of the U.S. east of the Continental Divide to determine the percentage of growing seasons with severe hail days above this threshold. RMA crop-hail insurance data were used as a supplement to the SVRGIS to define the agricultural regions of interest for crop-hail loss. Multiple RMA crop-hail insurance data metrics were computed for May–October during each year in the 1990–2020 period, including the 1) CPI-adjusted (2023 USD) mean payment indemnity for hail; 2) mean crop-hail loss cost; 3) mean percentage of insured crop acres that are damaged by hail in the growing season; and 4) the fraction of crop-hail loss out of all the RMA weather- and climate-related hazards (drought, excessive moisture, flood, freeze, frost, hot wind, excessive wind, heat, tornado, cold wet weather).

Modeled historical cropland, historical baseline cropland, and projected cropland data were used to compute changes (deltas) in cropland coverage within each county. First, the percentage of each county occupied by cropland was calculated. Then, changes were computed between 2005 and 1950, 2055 and 2005, and 2100 and 2005. Understanding the projected changes in cropland coverage with the updated crop-hail climatology helped define critical regions of interest for the following analyses.

2) HAIL IMPACT MONTE CARLO

The Hail Impact Monte Carlo (HailMC) model (Childs et al. 2020), adapted from Tornado Impact Monte Carlo (TorMC) (Strader et al. 2016), was used to investigate the statistical probabilities of hail impacting cropland under each future scenario. Previous literature used the TorMC to quantify the impacts of population and tornadoes on the human and built environment, and the model proved to be valuable in assessing the potential future changes in population exposure to tornadoes across the CONUS (Strader et al. 2016, 2017a,b). Indeed, infrastructure risk is different from assessing cropland risk, as the latter fluctuates depending on phenological stage timing, while the former remains relatively constant through the year. Still, using HailMC is appropriate when analyzing crop-hail impacts, provided that the timing of crop risk is thoroughly recognized and supplemented with phenological context. The HailMC model ingests historical hail swath data from the SVRGIS database that consists of the initial and end points of a hail swath. The model also ingests a controlled weighting surface that represents the spatial probability of severe hail occurrences over the growing season based on the historical distribution of reports over the 1990–2020 control period for each region of interest. A cost surface raster (cropland) is also used in the model as the exposure layer. The HailMC model simulated 5000 years—representing a balance of computational efficiency with distributional smoothness in modeled output—for four equal-area regions: northern Great Plains, southern Great Plains, Midwest, and South (Fig. 1). Exposure statistics were computed by using simulated hail swaths to understand the statistical probability of exceedance (POE) of annual cropland area impacted by hail swaths in

Authenticated lbundy@niu.edu | Downloaded 09/03/26 01:39 PM UTC

each study region, cropland area impacted per hail swath, and the percentage of each hail swath that is cropland.

3) Future exposure and risk

The final part of the analysis used WRF-BCC future hail projection data to calculate the mean number of severe hail days over 14 complete boreal summer growing seasons (May–October) in the HIST, MID, and END periods. To quantify the projected changes in hail risk, severe hail day changes were calculated between the HIST and MID periods and the HIST and END periods using both RCPs. All changes were calculated on a 10× coarsened grid and aggregated to the county level. Statistically significant differences between HIST and the four future periods were assessed using a Mann–Whitney U test at the 95% significance level (p value < 0.05). Finally, to visualize changes in both risk and exposure (severe hail days and cropland), a bivariate analysis of the percent changes in cropland area and percent changes in severe hail days was performed to determine whether there were any coherent trends in risk and exposure by region. Bivariate plots were created by pairing county-level severe hail day percent changes for MID and END with cropland percent changes for each SRES scenario, respectively. Here, positive percent changes in cropland area and severe hail days refer to changes $> 20\%$, negative changes in both variables refer to changes $< -20\%$, and small changes refer to differences in either variable between -20% and 20%. The use of slightly higher or lower thresholds did not notably impact the results.

4) Limitations and considerations

This study employs a novel framework that integrates dynamically downscaled, convection-permitting regional climate simulations with spatially explicit cropland projections to assess the future risk landscape of crop-hail impacts. While this approach enables a more comprehensive evaluation of agricultural exposure to severe hail, several considerations should be noted when interpreting the results.

First, IPCC climate forcing scenarios (RCPs) are combined with IPCC land-use scenarios (SRES), which originate from different modeling frameworks. Although the SRES scenarios have been superseded by more recent IPCC frameworks, the FORE-SCE datasets used here remain among the few spatially explicit, high-resolution, long-term land-use datasets available for the CONUS and continue to be widely applied in land-use change studies (e.g., Flanagan et al. 2021; Montefiore et al. 2023; Jain et al. 2025). As such, they provide a valuable resource for assessing plausible changes in cropland exposure over time, incorporating both socioeconomic drivers of demand and biophysical characteristics to determine land-use suitability (Jain et al. 2025). However, the socioeconomic assumptions underlying SRES scenarios may not fully reflect current or emerging policy, technological, and demographic trajectories, and regional land-use outcomes may differ under newer frameworks.

Importantly, the use of SRES and RCP scenarios in parallel is intentional. Cropland projections derived from SRES scenarios (A1B, A2, B1, and B2) are applied independently of the climate forcing scenarios (RCP4.5 and RCP8.5) used to assess severe hail. This approach isolates the influence of land-use change (cropland exposure) from changes in the hazard (hail risk) itself, providing a sensitivity-based framework to evaluate their relative contributions to agricultural impacts. While these scenario families are not directly coupled, approximate correspondences exist (e.g., RCP4.5 with SRES B1, RCP6.0 with A1B, and RCP8.5 with A2; Moss et al. 2010; IPCC 2014; van Vuuren and Carter 2014; Jones and O'Neill 2016; Abram et al. 2019). Using both frameworks in parallel ensures a wide sampling of plausible socioeconomic and climate futures, making the findings more robust rather than less, as demonstrated with prior research (e.g., Kloster et al. 2012; Sohl et al. 2019; Montefiore et al. 2023; Gaines et al. 2024). Notably, scenarios most consistent with current policy trajectories are best approximated by intermediate pathways, approximated here by RCP4.5 to RCP6.0 and most closely aligned with the A1B storyline. While B2 may also capture aspects of regionally oriented development, B1 likely represents a more optimistic sustainability pathway, whereas A2 and RCP8.5 are better interpreted as upper-bound scenarios rather than the most likely policy outcome (Climate Action Tracker 2025).

The use of RCP scenarios is also consistent with the WRF-BCC modeling framework employed herein. These simulations were developed and initialized using CMIP5 and were not designed to incorporate the newer shared socioeconomic pathway (SSP) framework (Gensini et al. 2023). While SSPs integrate socioeconomic development with emission trajectories, RCPs describe greenhouse gas concentrations and associated radiative forcing (Moss et al. 2010; Riahi et al. 2017; Meinshausen et al. 2020). Comparisons between CMIP5 RCP scenarios and their CMIP6 SSP counterparts (e.g., RCP4.5 vs SSP2-4.5 and RCP8.5 vs SSP5-8.5) indicate broadly similar climate responses, particularly through the midtwenty-first century (Abram et al. 2019; Tebaldi et al. 2021). Thus, the continued use of RCPs remains appropriate for regional climate impact analyses and facilitates comparison with the extensive CMIP5-based literature.

Additional considerations relate to the representation of agricultural systems. The cropland projection datasets used here do not distinguish between individual crop types, limiting the ability to assess commodity-specific hail impacts. However, total cropland extent captures the dominant spatial signal of agricultural exposure and provides a robust estimate of where severe hail intersects with cultivated land. Furthermore, this study does not explicitly account for crop phenology. As a result, the findings represent aggregate exposure-based risk rather than crop-specific damage potential. However, crop phenology and development timing will be discussed throughout.

Taken together, these considerations do not detract from the core findings but instead provide important context for their interpretation. Rather than precise forecasts, the results should be viewed as scenario-based assessments of how evolving land-use patterns and climate conditions may interact to shape future agricultural hail risk. This framework establishes a foundation for future work that could incorporate crop-specific distributions, phenological timing, and next-generation

Authenticated lbundy@niu.edu | Downloaded 09/03/26 01:39 PM UTC

scenario datasets to further refine estimates of climate-related agricultural impacts.

3. Results and discussion

a. Crop-hail risk

Results here reaffirm that the Great Plains (northern and southern plains combined; Fig. 1) is the most at risk for crop-hail damage and associated production loss (Fig. 2; Table 1). Major crops in this high-risk region include corn, cotton, sorghum, soybean, and wheat (supplemental Fig. 2), with other minor-producing crops, consisting of barley, oats, rye, peanuts, sunflowers, and millet, also exposed (NASS 2024). During the May–October growing season, many counties in Kansas, eastern Colorado, and western Nebraska average over seven severe hail days, while most of the Great Plains experience at least three (Fig. 2a). From 1990 to 2020, 77% of counties in the Great Plains recorded more severe hail days than the eastern CONUS average (3 days) in 80% of growing seasons (Fig. 2b).

Severe hail risk declines eastward into the Midwest and South, where most counties experience one to three severe hail days per growing season. Even with the relatively lower hazard frequency compared to the Great Plains, these regions still contain extensive areas of corn, cotton, soybean, and wheat cultivation (supplemental Fig. 2), resulting in substantial exposure and potential for impactful losses. Specialty crops, particularly fruits and vegetables in the Midwest and fruits, vegetables, and tobacco in the South, are also highly exposed if unprotected (NASS 2024). Less than half of the growing seasons in these regions exceeded the CONUS mean of three severe hail days for most counties over the 1990–2020 period, underscoring the primary concentration of climatological hail risk in the Great Plains. Seasonally, hail events peak during May and June, with a gradual decline in both magnitude and frequency through July and onward (Cintineo et al. 2012; Allen et al. 2015). While risk remains elevated across the Great Plains by September and October, it diminishes in the Midwest and South by the late season, coinciding with the primary harvest period.

In relating climatological hail risk to agricultural loss, crop-hail insurance data highlight extensive vulnerability across the western Great Plains (Figs. 2c–f), consistent with prior studies (e.g., Reyes and Elias 2019; Reyes et al. 2020; Bundy et al. 2022). During the growing season, mean indemnity payouts exceed \$260,000 USD in more than two-thirds of the region, with loss costs surpassing \$2.50 per \$100 of liability. Payments in the Great Plains are at least 150% higher than in the Midwest or South, reflecting both elevated climatological risk (Table 1) and broader insurance dynamics (Young et al. 2001; Coble and Barnett 2013). In several western Great Plains counties, at least 5% of insured acreage is damaged by hail, with hail accounting for more than 40% of all weather-related indemnities in the region per growing season.

Hail frequency and magnitude vary through the summer growing season, with crop losses strongly dependent on phenological timing (supplemental Fig. 3). Although May ranks among the highest for severe hail occurrence (second only to June), corn indemnities are generally lower in May across the Great Plains and Midwest because most plants are still in the emergence stage and can often recover from damage (Vorst 1993; Lindsey et al. 2024). The South is an exception, as corn there is typically further along in the vegetative stage, making recovery less likely and yield losses more severe. Once corn reaches tasseling and silking, yield losses can approach 100%, underscoring the crop's heightened vulnerability even when climatological hail risk declines later during the summer (Changnon et al. 2009). Vulnerability declines from August through October as kernels mature, with decreasing risk of yield loss and indemnities from hail (Battaglia et al. 2019).

Other crops contain similar stage-specific vulnerabilities. Soybeans are most vulnerable in the late vegetative, flowering, and pod-fill periods, typically July–August, when even moderate hail can cause severe losses despite the lower climatological frequency (supplemental Fig. 3; MacMillan 2023). Cotton is most vulnerable during emergence and squaring (May–June), coinciding with peak hail occurrence, but also faces damage in the open boll stage in September–October, especially throughout the southern plains and South (Yue et al. 2019). Wheat losses mirror corn, with damage during the milk and hard dough stages (May–July) causing major yield reductions (Katz and Garcia 1981; Childs et al. 2020; Lindsey et al. 2024). While the hail climatology does not always align with the most critical phenological stages, windows of significant vulnerability exist for all major crops, underscoring the importance of aligning coverage strategies with phenological risk windows rather than treating hail as a uniform seasonal hazard.

b. Cropland exposure

Spatiotemporal changes in exposure have often been overlooked as drivers of disaster risk (Bouwer 2011), and while not completely analogous to potential changes in agricultural exposure risk, recent work demonstrated that shifts in urban, suburban, and exurban development have amplified disaster potential (Ashley and Strader 2016). Historical cropland changes are well documented (supplemental Fig. 4; Lark et al. 2015; Yu and Lu 2018; Lark et al. 2020), but future agricultural landscapes remain uncertain and will be shaped by societal, environmental, and economic trajectories. Furthermore, cropland extent will be influenced by suburban and exurban expansion (Sohl et al. 2018a), conservation policies (Nakicenovic et al. 2000; Lark et al. 2020), and evolving land-use pressures such as wind and solar energy development (Mai et al. 2021; Harrison-Atlas et al. 2022; Goldberg 2023).

Future cropland coverage is projected to vary regionally from the historical baseline period through the mid- and end of century (Figs. 3 and 4; Table 2). County-level cropland changes across IPCC SRES scenarios display the most pronounced changes in the Great Plains, coinciding with the nation's highest climatological hail risk and crop-hail loss potential. In 2005, cropland accounted for 37% (85 million acres) of northern plains land area and 21% (49 million acres)

Authenticated lbundy@niu.edu | Downloaded 09/03/26 01:39 PM UTC

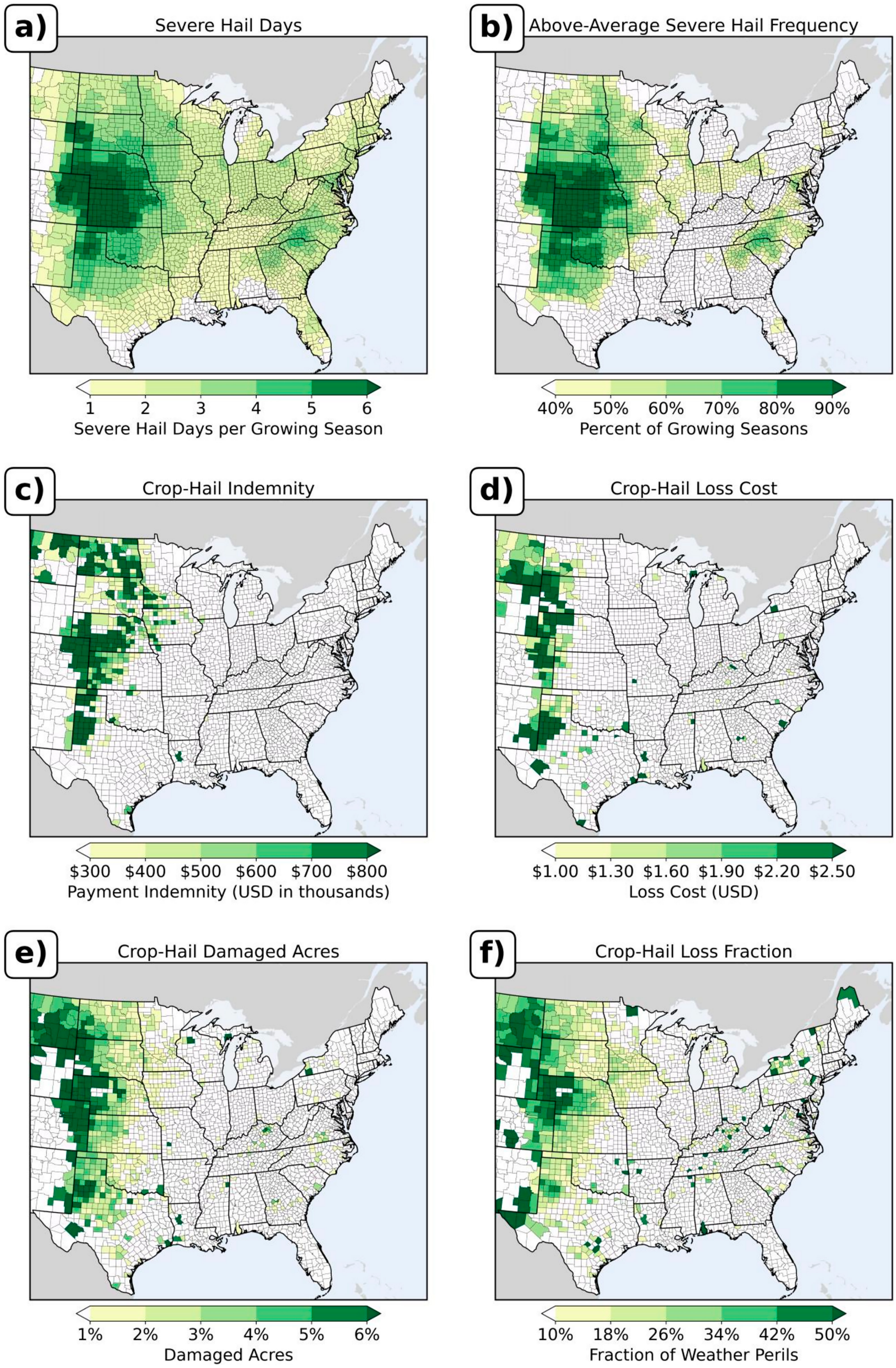

FIG. 2. County-level crop-hail climatology over the May–October 1990–2020 period, showing (a) mean number of severe hail days per growing season; (b) percentage of growing seasons with above national (east of the U.S. Continental Divide) county-level mean number of severe hail days; (c) mean growing season CPI-adjusted (2023 USD) payment indemnity due to crop-hail damage; (d) mean crop-hail loss cost (indemnity/liability × 100); (e) mean percentage of insured cropland damaged by hail per growing season; (f) mean fraction of weather peril crop loss caused by hail per growing season.

Authenticated lbundy@niu.edu | Downloaded 09/03/26 01:39 PM UTC

TABLE 1. Crop-hail county-level climatological means per growing season as in Fig. 1, but averaged by region.

Region	Severe hail days	Above-average severe hail seasons (%)	Crop-hail payment indemnity	Crop-hail loss cost	Crop-hail damaged acres (%)	Crop-hail loss fraction (%)
Northern plains	5	71	$620,796	$0.85	3.24	26.15
Southern plains	5	68	$569,600	$0.88	2.59	17.27
Midwest	3	44	$86,276	$0.09	0.54	7.57
South	2	30	$32,705	$0.25	0.51	7.49

of southern plains land (Figs. 3a and 4a). By 2055, cropland coverage is projected to increase by as much as 5% in the northern plains and 8% in the southern plains, with increases reaching 18% by 2100 in both regions relative to 2005 (Figs. 3 and 4; Table 2). Under the most aggressive storylines (A1B and A2), cropland may comprise up to 55% of the northern plains and 39% of the southern plains by the century's end. At the county scale, cropland coverage is projected to rise by ≥5% in 28% of Great Plains counties by 2055 and by ≥10% in 40% of counties by 2100. All four scenarios suggest an increase in southern plains cropland by 2055, while only B2 suggests a slight decline in the northern plains. This expansion could be consequential given evidence that newly converted lands in the region often yield below-average returns for corn, soybeans, and wheat compared to existing cropland in the region (Lark et al. 2020). These reduced returns stem from declining crop conditions (Bundy et al. 2024) and a lower harvest-to-planting ratio with high interannual variability (supplemental Fig. 5).

In the Midwest, cropland accounted for 45% (91 million acres) of total land area in 2005—the highest of any U.S. region. Future changes are projected to be minimal, as two scenarios (A1B and A2) suggest slight increases, while the other two (B1 and B2) display modest declines by 2055 and 2100 (Figs. 3 and 4; Table 2). Overall, with nearly half of the land area in cultivation already, cropland exposure in the Midwest is unlikely to shift substantially through the century. In contrast to the Midwest, only 15% of land in the South was cropland in 2005, and scenario divergence is greatest in the South. As such, A1B and A2 project increases of 13%–17% by 2055 and up to 72% by 2100, whereas B1 and B2 indicate decreases of 18%–31% by 2055 and up to 40% by 2100, reflecting differing socioeconomic and land-use assumptions embedded within the SRES scenario families and highlighting uncertainty in future cropland trajectories across the South. Overall, these regional and scenario-dependent differences demonstrate that future agricultural exposure may increase or decrease substantially depending on land-use pathway, underscoring the need to evaluate both cropland expansion and contraction across hail-prone regions. In sum, A1B and A2 generally project cropland expansion by 2055 and 2100, with the largest increases occurring in the northern and southern plains, while B1 and B2 project smaller changes. Scenario divergence is most pronounced by 2100, especially in the Great Plains and South, where A2 produces the greatest cropland expansion, whereas B2 often indicates cropland contraction. Such exposure changes are critical for understanding future production loss risk and may parallel how disaster potential emerges from expansion of the human footprint and property into hazard-prone areas (e.g., Pielke 2005; Pielke et al. 2008; Simmons et al. 2013; Ashley and Strader 2016).

c. *Interaction of hail risk with changing cropland exposure*

Changes in cropland coverage directly affect the acreage vulnerable within a hail swath, reflecting the expanding bull's-eye effect observed in human exposure to weather hazards (Ashley et al. 2014; Rosencrants and Ashley 2015; Ashley and Strader 2016; Strader et al. 2017a,b, 2018). As such, changes in exposure need to be evaluated by varying cropland coverage while holding hail hazard characteristics constant. This changing dynamic is evident in western Kansas, eastern Colorado, and western Nebraska, where all IPCC SRES scenarios project cropland expansion between 2005 and 2100 (Fig. 5). To illustrate how this expanding exposure translates into increased agricultural risk, 500 years of the 5000-yr HailMC simulation reveal hail impacts on cropland increasing by 79%—from approximately 990 000 acres in 2005 to 1.7 million acres under the A2 2100 scenario (Fig. 5). Key crops in this high-risk corridor include corn, soybeans, sorghum, winter wheat, and several minor crops, such as millet, peas, rye, beans, and sunflowers (NASS 2024). These results indicate an increasing probability of crop-hail losses as exposure grows, even if hazard frequency remains constant. While this regional example highlights the mechanics of the agricultural expanding bull's-eye effect, a comprehensive understanding of future crop-hail risk requires broader regional analyses. Thus, the variability in crop-hail impacts depends significantly on regional differences and the timing of the most vulnerable phenological stages.

Across the 5000-yr HailMC simulation, a total of 485 464 severe hail swaths were generated over the northern plains, southern plains, Midwest, and South. The southern plains averaged the most swaths per growing season (28), followed by the Midwest (27), northern plains (26), and South (16). Swath dimensions were relatively consistent (mean length around 9.8 km, mean width of 1.25 km), though mean hail size varied: 1.8 in. (4.57 cm) in the Great Plains, 1.6 in. (4.06 cm) in the Midwest, and 1.4 in. (3.56 cm) in the South (Table 3). POE curves illustrate how historical and future cropland extent and the historical hail climatology shape growing-season impacts (Figs. 6 and 7). During the historical baseline (2005), mean cropland area impacted per season was highest in the Midwest (37 170 acres), followed by the northern plains (28 430 acres), southern plains (22 910 acres), and South (7760 acres) (Fig. 6; Table 4). While not all impacts result in

Authenticated lbundy@niu.edu | Downloaded 09/03/26 01:39 PM UTC

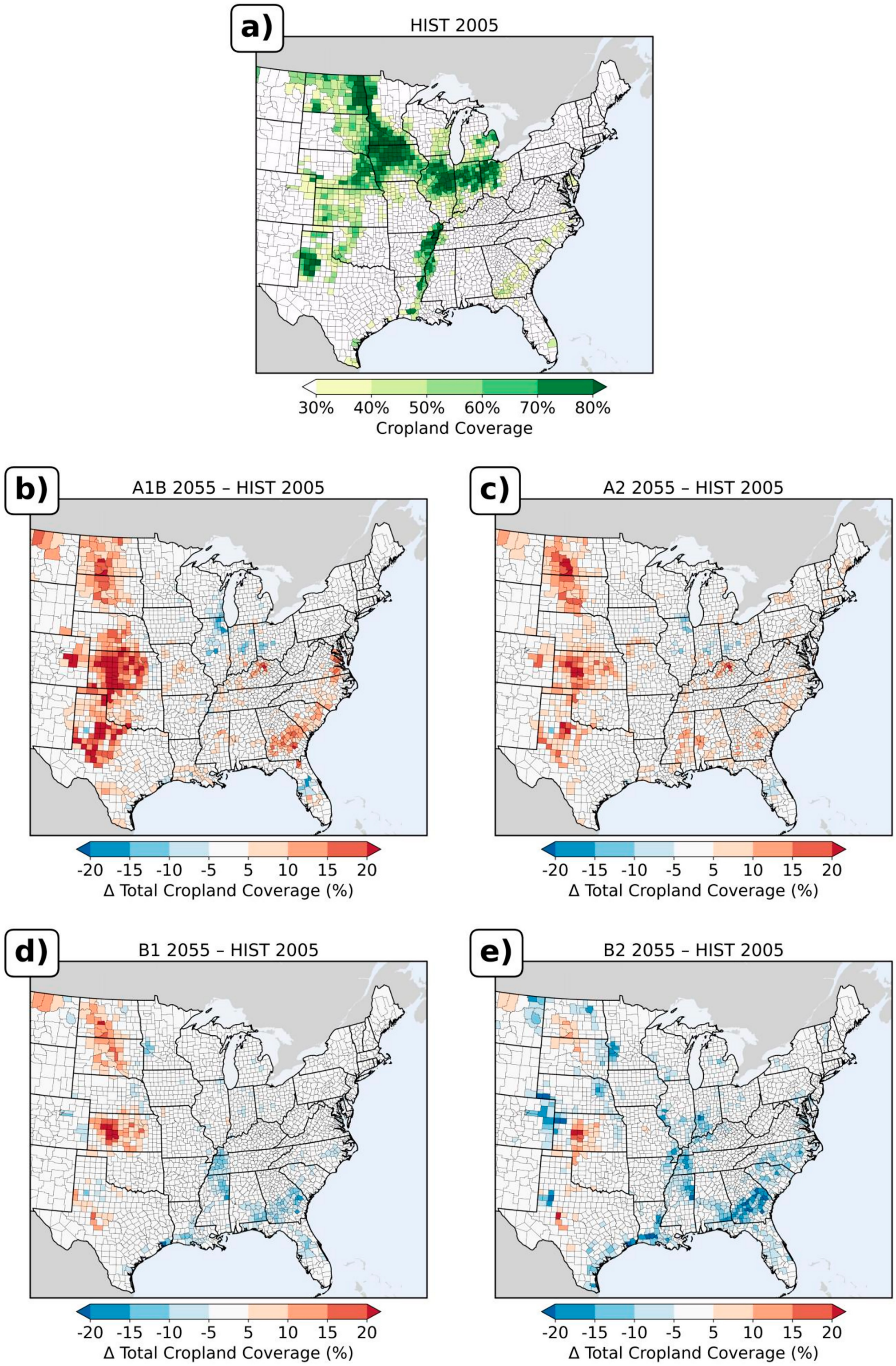

FIG. 3. (a) Percentage of each county classified as cropland in 2005; (b)–(e) changes in cropland percentage between 2055 and 2005 for each IPCC SRES scenario.

Authenticated lbundy@niu.edu | Downloaded 09/03/26 01:39 PM UTC

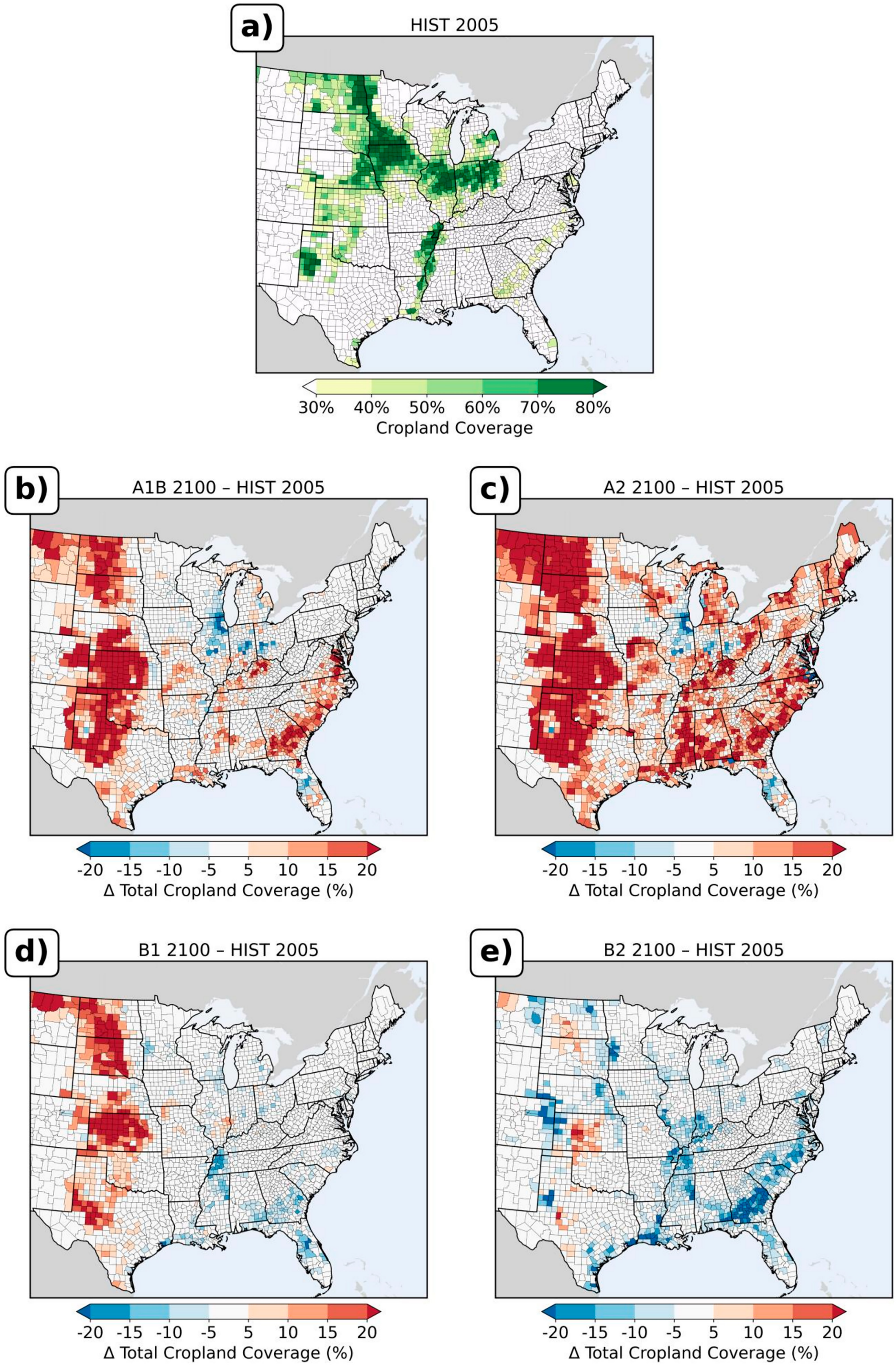

FIG. 4. As in Fig. 3, but for 2100.

Authenticated lbundy@niu.edu | Downloaded 09/03/26 01:39 PM UTC

TABLE 2. Changes in the percentage of land area classified as cropland by region for 2055 relative to 2005 and for 2100 relative to 2005 for all IPCC SRES scenarios (A1B, A2, B1, B2).

	2055				2100			
	A1B	A2	B1	B2	A1B	A2	B1	B2
Northern plains	5.44	4.28	1.75	−1.96	10.95	18.17	7.88	−2.61
Southern plains	7.74	4.55	2.09	0.07	14.37	17.81	7.12	−0.11
Midwest	0.07	1.10	−0.95	−2.65	0.53	5.88	−0.48	−3.54
South	2.15	2.66	−2.93	−4.76	4.42	11.22	−2.86	−6.28

outright yield loss, hail can reduce crop quality and marketability at any growth stage with a varying magnitude, underscoring its persistent threat to agricultural productivity (Bundy et al. 2024; Lindsey et al. 2024).

Across individual SRES scenarios, most mid- and end-of-century regional mean crop-hail impacts remain below the historical Midwest mean of about 37 000 acres impacted per growing season (Figs. 6 and 7; Table 4). Only the northern plains under A2 in 2100 (about 42 000 acres) and the southern plains under A1B and A2 in 2100 (about 38 000 and 41 000 acres, respectively) exceeded this historical Midwest benchmark. At the swath scale, Midwest cropland exposure was already substantial in 2005, with over 1300 affected acres per severe hail swath and accounting for 46% of the swath area on average. This baseline exposure exceeded the projected 2055 and 2100 values for every other region, highlighting the Midwest's uniquely high concentration of cropland within severe hail swaths (supplemental Figs. 6 and 7; supplemental Tables 1 and 2). With 45% of its land already cropland, the

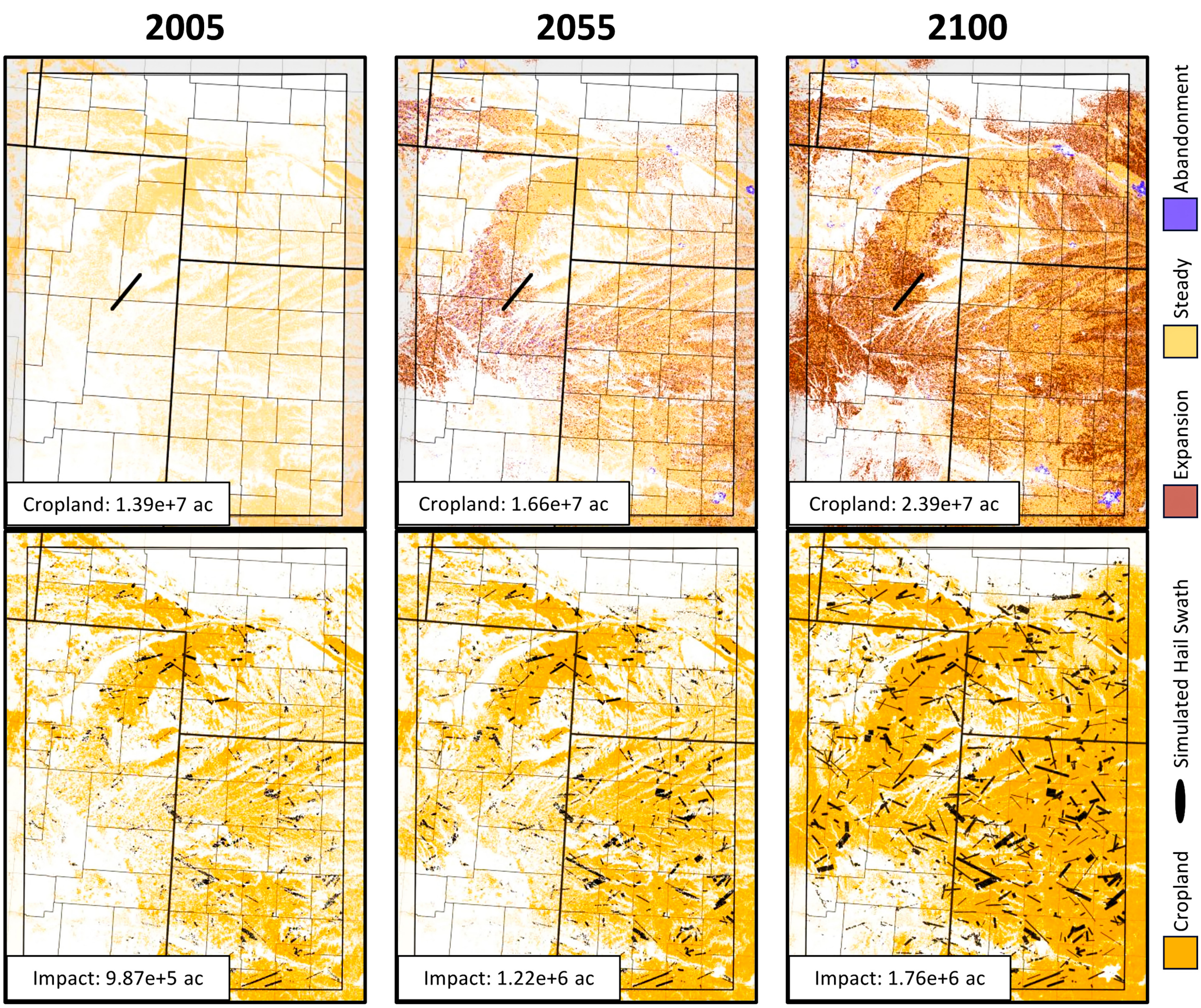

FIG. 5. Example HailMC simulation over eastern Colorado, western Kansas, and western Nebraska showing historical (2005) and projected A2-scenario cropland exposure surface for 2055 and 2100. (top) Cropland extent for each period, with cropland expansion relative to 2005 displayed in red and cropland abandonment in blue; the black line denotes a single example simulated hail swath. (bottom) Cropland (orange) and hail swaths (black) simulated using 500 years drawn from the 5000-yr HailMC simulation, with swaths shaded by their relative cropland impact (darker swaths indicate greater impact). Insets report total cropland area in the top panels and total impacted cropland area in the bottom panels.

Authenticated lbundy@niu.edu | Downloaded 09/03/26 01:39 PM UTC

TABLE 3. Summary statistics by region of the 5000-yr HailMC simulation.

Region	Simulation swath total	Mean annual swath total	Mean swath width (km)	Mean swath length (km)	Mean severe hail size (mm)
Northern plains	130 704	26.14	1.25	9.80	45.82
Southern plains	137 904	27.58	1.25	9.79	45.36
Midwest	136 589	27.32	1.25	9.83	39.96
South	80 267	16.05	1.25	9.79	34.63
National	485 464	97.09	1.25	9.81	42.19

Midwest is the most exposed region to hail, though this has not historically produced losses on par with the Great Plains. At the upper end of the annual impact distribution, however, the southern plains consistently exceeds the Midwest. Here, the 95th and 99th percentiles represent the cropland area intersected by simulated hail swaths during the most impactful 5% and 1% of growing seasons, respectively. In 2005, the southern plains 95th-percentile impact was approximately 94 000 acres, which was over 10 000 acres (13%) greater than the Midwest value of ~83 500 acres. At the 99th percentile, the corresponding values were almost 127 000 and 107 000 acres, a difference of about 20 000 acres (18%). Across the 2055 scenarios, southern plains 95th-percentile impacts range from almost 97 000 to 131 000 acres, exceeding the corresponding Midwest values by about 16 500–48 000 acres (21%–58%). By 2100, this difference increases to almost 17 000–83 000 acres (21%–93%). These extreme annual impacts occur when multiple, large, or favorably positioned hail swaths

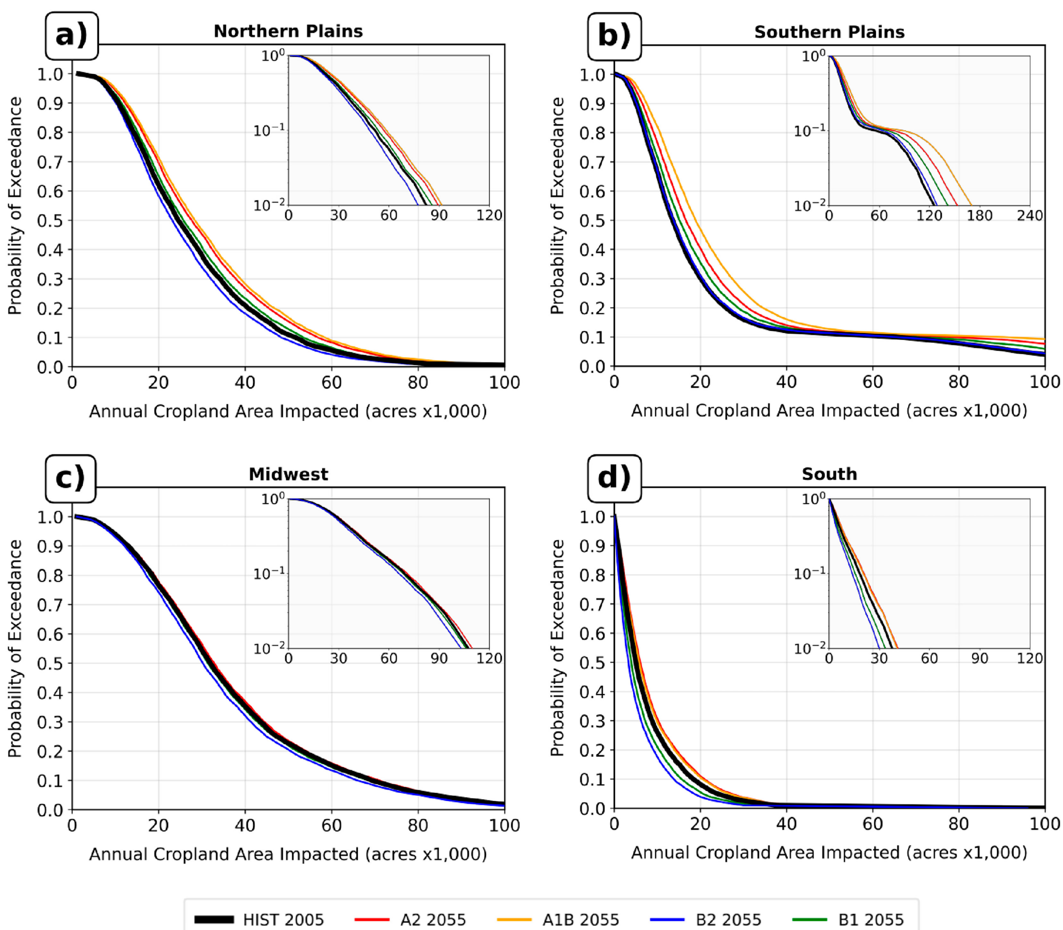

FIG. 6. POE curves comprising a 5000-yr HailMC simulation of the 2005 annual cropland area impacted by severe hail (solid black line), the 2055 annual cropland area impacted by severe hail for each IPCC SRES scenario (A1B, A2, B1, B2) by region: (a) northern plains, (b) southern plains, (c) Midwest, and (d) South. Each panel contains a subplot of the same POE curves with a log (y) axis.

Authenticated lbundy@niu.edu | Downloaded 09/03/26 01:39 PM UTC

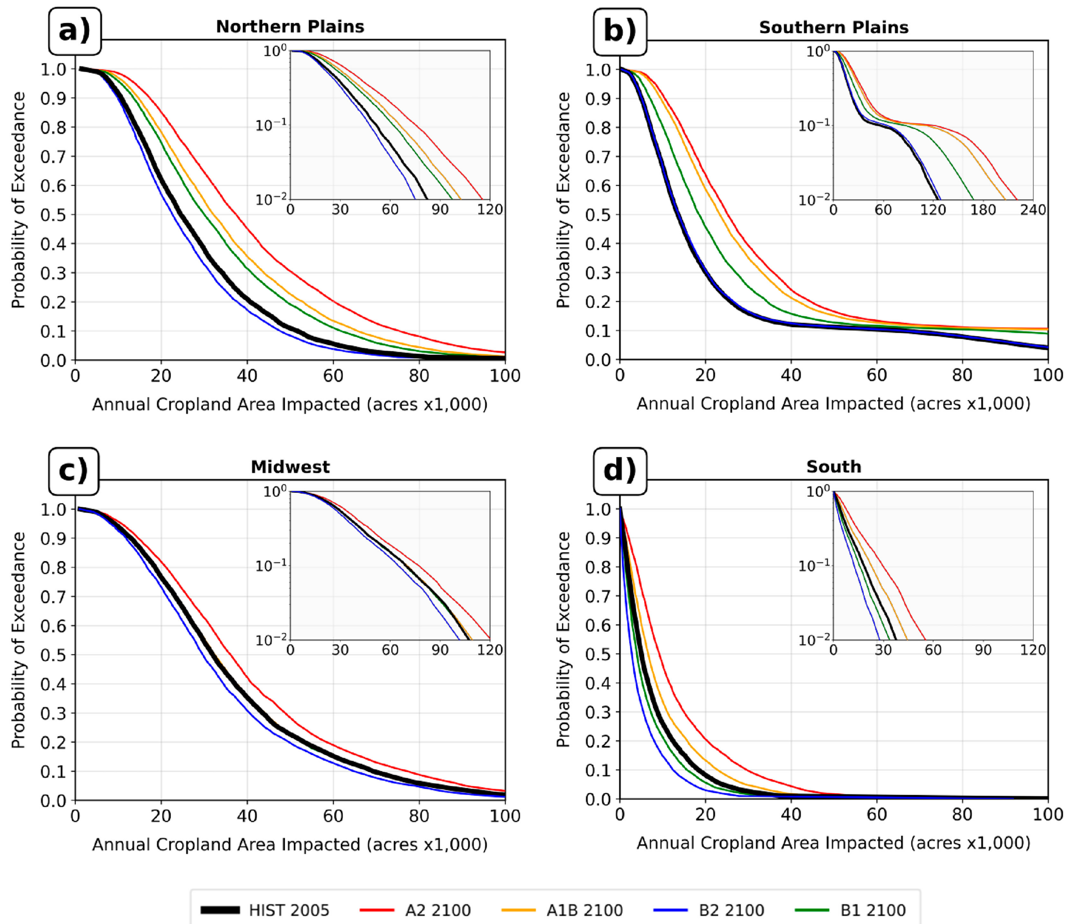

FIG. 7. As in Fig. 6, but for the 2100 cropland projections.

overlap extensive and contiguous areas of cropland. Therefore, although mean impacts are larger in the Midwest, the southern plains has greater potential for rare, high-impact crop-hail seasons because its cropland more frequently overlaps the climatological maximum in severe hail activity.

The northern and southern plains are the only regions where at least three of the four land-cover projections exhibit increases in mean crop-hail impacts by both the mid- and end of century (Figs. 6 and 7; Table 4; supplemental Figs. 6 and 7; supplemental Tables 1 and 2). In the southern plains, mean impacted acreage increases from approximately 23 000 acres in 2005 to ~23 400–31 600 acres in 2055, representing absolute increases of approximately 400–8600 acres (2%–38%). By 2100, mean impacts range from approximately 23 200 to 41 600 acres, representing increases of nearly 300–18 700 acres (1%–81%). In the northern plains, mean impacts change from about 28 000 acres in 2005 to 27 000–33 000 acres in 2055, equivalent to changes from −6% to +15%. By 2100, projected impacts range from approximately 26 000 to 42 000 acres, corresponding to changes from −2000 to +14 000 acres (from −8% to +49%). The largest increase occurs under A2 in 2100, when about 14 000 additional acres are impacted per growing season, a 49% increase relative to 2005.

Although the Midwest has historically had the greatest cropland exposure to hail, this exposure is not projected to change significantly by mid- or end of century, as most available land is already in cultivation (Figs. 6c and 7c; Table 4). Relative to the 2005 mean of ~37 000 acres, projected Midwest impacts range from about 35 000 to almost 38 000 acres in 2055, representing changes from −2000 to +1000 acres (from −5% to +2%). By 2100, impacts range from ~34 500 to 41 500 acres, corresponding to changes from −7% to +11%. Similar stability is evident for acres impacted per swath and the percentage of each swath intersecting cropland (supplemental Figs. 6 and 7; supplemental Tables 1 and 2), indicating limited sensitivity to future land-cover change in this already highly cultivated region. In the South, where cropland exposure and crop-hail impacts are lowest, projections diverge more sharply among scenarios. Relative to the 2005 mean of almost 8000 acres, projected impacts in the South range from approximately 5600 to 9000 acres in 2055, representing changes from −2200 to +1200 acres (from −28% to +16%). By 2100, impacts range from approximately 4900 acres under B2 to 13 000 acres under A2, corresponding to changes of −2800 acres (−36%) and +5200 acres (+67%), respectively. Thus, although the South exhibits comparatively large percentage changes, its

Authenticated lbundy@niu.edu | Downloaded 09/03/26 01:39 PM UTC

TABLE 4. Regional cropland area impacted (in thousands of acres) by severe hail per growing season from the 5000-yr HailMC simulation, using HIST (2005) cropland coverage and IPCC SRES cropland projections (A1B, A2, B1, B2) for 2055 and 2100.

	HIST	A1B		A2		B1		B2	
	2005	2055	2100	2055	2100	2055	2100	2055	2100
Northern plains									
Mean	28.43	32.63	36.90	31.73	42.48	29.74	34.47	26.77	26.21
95th percentile	61.37	69.35	77.75	67.71	88.36	63.48	72.74	57.42	56.13
99th percentile	82.26	91.64	102.54	89.43	115.49	85.82	97.42	77.41	75.07
Southern plains									
Mean	22.92	31.58	38.48	28.02	41.57	25.57	30.93	23.36	23.23
95th percentile	94.19	130.98	160.89	115.91	173.66	105.27	127.46	96.75	95.65
99th percentile	126.87	170.49	206.90	153.26	220.93	141.99	168.59	129.18	129.12
Midwest									
Mean	37.18	37.20	37.51	37.97	41.44	36.51	36.94	35.23	34.56
95th percentile	83.55	82.87	83.55	84.51	90.72	82.25	83.01	80.18	78.83
99th percentile	107.39	107.09	109.36	109.74	120.72	106.13	107.36	103.06	101.66
South									
Mean	7.77	8.75	9.79	8.99	13.01	6.43	6.46	5.60	4.94
95th percentile	23.87	26.63	29.29	27.17	38.62	20.51	20.82	18.49	16.93
99th percentile	37.68	40.65	44.48	41.18	55.42	33.58	33.75	29.97	27.75

absolute impacts remain substantially smaller than those in the Great Plains and Midwest. Taken together, the Great Plains emerge as the region where cropland expansion most strongly amplifies hail exposure, while the Midwest remains comparatively stable and the South exhibits high scenario uncertainty but lower absolute crop-hail impacts. These contrasts highlight that future crop-hail risk may be shaped more by land-use change than hazard frequency alone, with significant implications for insurance portfolios, farm management, and regional adaptation planning.

d. Changing hail risk with changing cropland exposure

While cropland exposure may shift regionally, hail risk itself is not expected to remain constant through the twenty-first century. Across all WRF-BCC scenarios (MID4.5, MID8.5, END4.5, and END8.5), statistically significant decreases in growing-season severe hail days are projected for the western Great Plains, though the extent and magnitude vary by emissions pathway and period (Fig. 8). The END8.5 scenario suggests the most widespread reductions, with 0.5–2.5 fewer severe hail days per growing season—a 33%–43% decline compared to HIST—centered on eastern Colorado, northeastern New Mexico, western Kansas, and central Nebraska (Fig. 8; Table 5; supplemental Fig. 8). Other scenarios contain decreases of similar magnitude but smaller spatial extent, as MID4.5 and MID8.5 reductions focus on the southern plains, while END4.5 extends farther north into Nebraska and South Dakota. Collectively, these projections suggest fewer severe hail days across much of the plains, pointing to a potential decline in future hail risk within the current climatological maximum, while also suggesting an increasing number of severe hail days across the broader eastern United States.

While growing-season projections provide a broad illustration, the timing of changes relative to crop phenology is critical for understanding future loss vulnerability. Although hail can reduce crop quality and yield at any stage, monthly trends determine which growth phases are most at risk. In the western southern plains, severe hail days are projected to decline across all growing-season months by the mid- and end of century (Gensini et al. 2024), benefitting vegetative and reproductive periods of corn, cotton, sorghum, and wheat. Although uncertainty remains because these projections are based on a single modeling framework, WRF-BCC simulations have been shown to explicitly resolve supercell structures and storm-scale processes relevant to severe hail production (Ashley et al. 2023; Gensini et al. 2024). Therefore, the reduction of severe hail in the western southern plains is largely tied to a projected decrease in supercell frequency, the dominant severe hail-producing storm type in the United States (Ashley et al. 2023). In the northern plains, July and later months display a general decline in severe hail days, but May and June exhibit slight increases, posing risks to crops during critical vegetative development stages (Gensini et al. 2024). Nonetheless, even if portions of the Great Plains experience a relative decline in severe hail frequency, the region is still projected to remain the climatological epicenter for hail risk in the United States.

Although projected declines in severe hail days suggest reduced future agricultural losses in the Great Plains (if cropland exposure is held constant), uncertainties remain regarding hail frequency and size (Raupach et al. 2021). Prior studies point to fewer hail days across parts of North America (Brimelow et al. 2017; Gensini et al. 2024), though changes may depend on hail size (Brimelow et al. 2017; Tang et al. 2019; Trapp et al. 2019). One driver is increased convective inhibition (CIN), which may suppress storm initiation or intensification; WRF-BCC and other simulations suggest stronger CIN across the Great Plains in future periods (Trapp and Hoogewind 2016; Hoogewind et al. 2017; Rasmussen et al. 2020; Haberlie et al. 2022, 2024; Ashley et al. 2023). Higher melting levels may also reduce smaller hailstones (Brimelow et al. 2017; Gensini et al. 2024). Yet, the

Authenticated lbundy@niu.edu | Downloaded 09/03/26 01:39 PM UTC

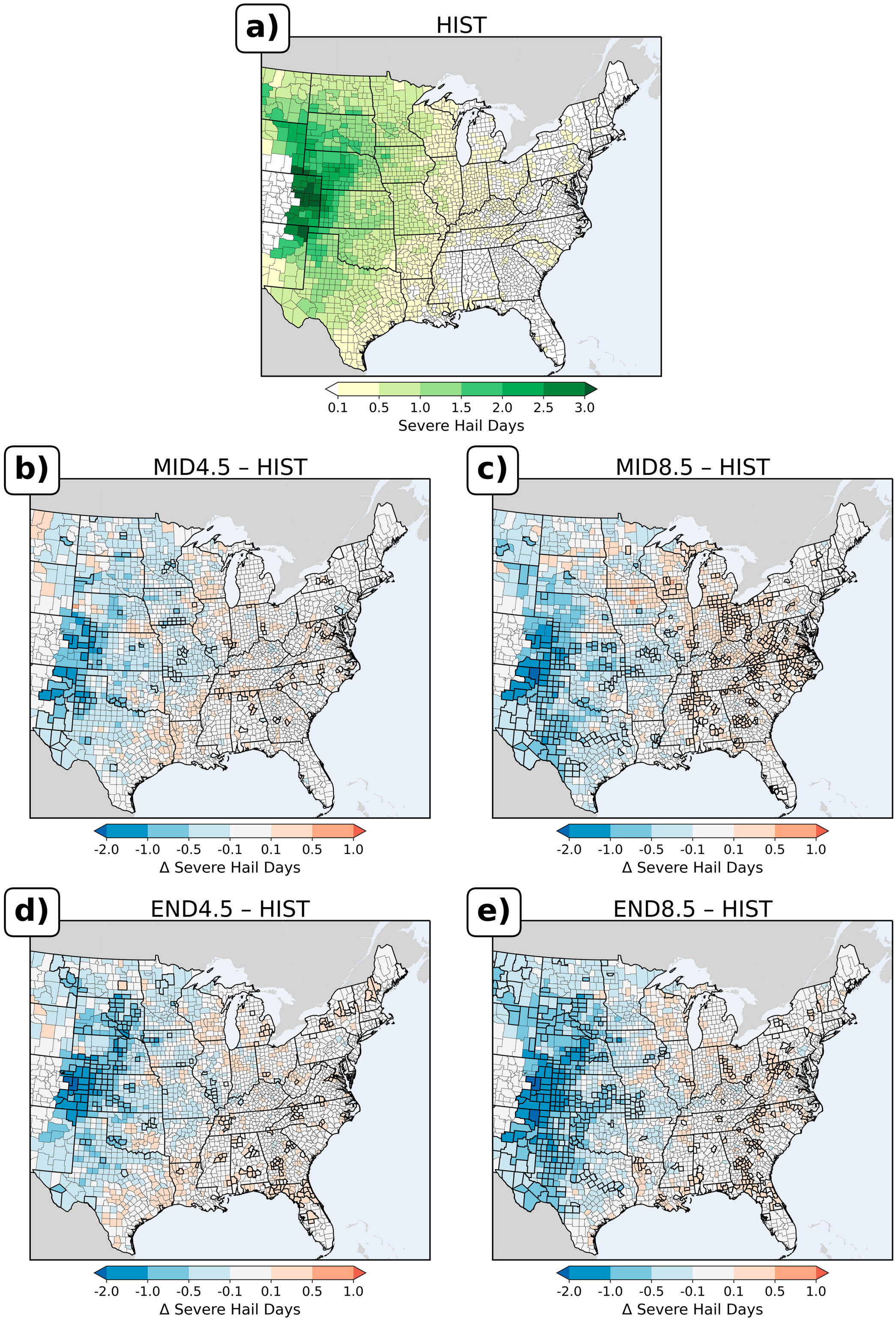

FIG. 8. (a) HIST mean growing-season severe hail days and changes in mean growing-season severe hail days relative to HIST for (b) MID4.5, (c) MID8.5, (d) END4.5, and (e) END8.5. Counties with statistically significant differences between HIST and the future periods are denoted by thick black outlines ($p < 0.05$; Mann–Whitney U test).

Authenticated lbundy@niu.edu | Downloaded 09/03/26 01:39 PM UTC

TABLE 5. Regional percent changes in severe hail days and cropland coverage relative to historical conditions. Severe hail changes are displayed for WRF-BCC MID4.5 and END8.5, while cropland changes are for each IPCC SRES scenario (A1B, A2, B1, B2).

		Severe hail percent change		Cropland percent change			
	Period	RCP4.5	RCP8.5	A1B	A2	B1	B2
Northern plains	MID	−13.39	−8.97	14.75	11.61	4.74	−5.32
Southern plains	MID	−22.45	−39.83	36.87	21.68	9.96	0.35
Midwest	MID	34.17	80.17	0.17	2.46	−2.13	−5.91
South	MID	427.67	737.76	13.80	17.06	−18.82	−30.57
Northern plains	END	−24.36	−33.35	29.69	49.27	21.38	−7.07
Southern plains	END	−20.88	−43.44	68.52	84.90	33.92	−0.55
Midwest	END	35.32	48.59	1.17	13.10	−1.07	−7.89
South	END	543.43	555.13	28.40	72.04	−18.36	−40.36

implications of these changes remain uncertain due to multiple factors, including the computational demands of explicitly simulating storms and hail microphysics, limitations in microphysical parameterizations (e.g., hail growth, melting, and size distributions), sensitivity to environmental inputs such as thermodynamic profiles and wind shear that vary across climate models, and observational constraints such as biases and spatial heterogeneity in hail reports. Additionally, when assessing the full spectrum of regional agricultural risk, projected declines in severe hail frequency across the Great Plains may coincide with reductions in spring and summer precipitation, raising broader concerns about climate change impacts on regional crop production.

East of the Mississippi River, most counties are projected to experience minimal changes or slight increases of less than one severe hail day per growing season (Fig. 8). Although small in absolute terms, these changes represent large relative increases—50% to more than 500% in parts of the eastern Midwest, South, mid-Atlantic, and Northeast—given the historically lower hail frequencies in these regions (Figs. 2a and 8a). MID8.5 displays the most widespread significant increases, particularly across the Midwest, South, and mid-Atlantic (Fig. 8). Importantly, these increases are concentrated in the first half of the growing season (Gensini et al. 2024), coinciding with vegetative and early reproductive stages of corn, cotton, and soybeans, when crops across these regions are especially vulnerable.

When hail risk is evaluated alongside cropland exposure, all combinations of RCP4.5 and RCP8.5 with the SRES storylines are considered; however, greater emphasis is placed on the RCP4.5/B1 and RCP4.5/A1B combinations because these represent the closest approximate parallels between the RCP and SRES frameworks and are most consistent with present-day policy trajectories (Figs. 9 and 10; Table 5). By midcentury, much of the northern and southern plains are projected to experience decreasing severe hail frequency but increasing cropland exposure relative to the historical period. This pattern persists into the end-of-century period, with larger reductions in severe hail days occurring alongside continued cropland expansion. Therefore, projections suggest that rising exposure may partially offset reductions in hazard frequency by sustaining, or in some cases increasing, crop-hail loss potential across the Great Plains. In the Midwest, simulations indicate increasing severe hail frequency across much of the region, while cropland coverage changes remain relatively small. The SRES A-family scenarios generally project modest cropland increases, whereas the B-family scenarios indicate modest decreases during both the mid- and end-of-century periods. Meanwhile, the South exhibits some of the largest projected increases in severe hail frequency, with regional average changes approaching 500% during both future epochs. These severe hail increases coincide with the greatest divergence among cropland scenarios: A-family scenarios project substantial cropland expansion, comparable in magnitude to changes in the northern plains, while B-family scenarios project substantial cropland contraction. Thus, although future exposure pathways remain highly uncertain in the South, the projected increase in severe hail frequency indicates a greater annual likelihood of crop exposure to severe hail. Additionally, while not a region of focus, the mid-Atlantic may experience concurrent increases in both severe hail frequency and cropland exposure, enhancing vulnerability to future crop-hail losses. However, given the comparatively smaller cropland footprint and lower historical hail risk relative to the Great Plains, the overall magnitude of impacts in the South and broader eastern United States is unlikely to match those projected for the primary hail-prone agricultural corridor.

Regional variation is important: The Great Plains face the greatest exposure-driven risk, while the Midwest and South may undergo hazard-driven increases with variable changes in cropland extent between scenarios. These dynamics carry clear implications for both policy and practice. Insurers will need to align coverage with shifting regional risk profiles (Chemeris et al. 2022; Obolensky 2025), while policymakers and sustainability programs may use conservation incentives and land-use planning to discourage expansion into marginal, hazard-prone lands (Lark et al. 2015; Farm Service Agency 2025). At the farm level, mitigation is most effective when approached as a layered strategy that integrates prevention, protection, and recovery. Preventive measures include climatological risk assessments (RMA 2025), early warning systems (NWS 2025), crop diversification (Renard and Tilman 2019), and the use of crop insurance as a financial safety net (Reyes and Elias 2019). Physical protections such as hail netting or wired caging are effective for high-value cropping systems but are cost-prohibitive at the scale of broadacre cropping systems (Bendorf and Schillerberg 2024).

Authenticated lbundy@niu.edu | Downloaded 09/03/26 01:39 PM UTC

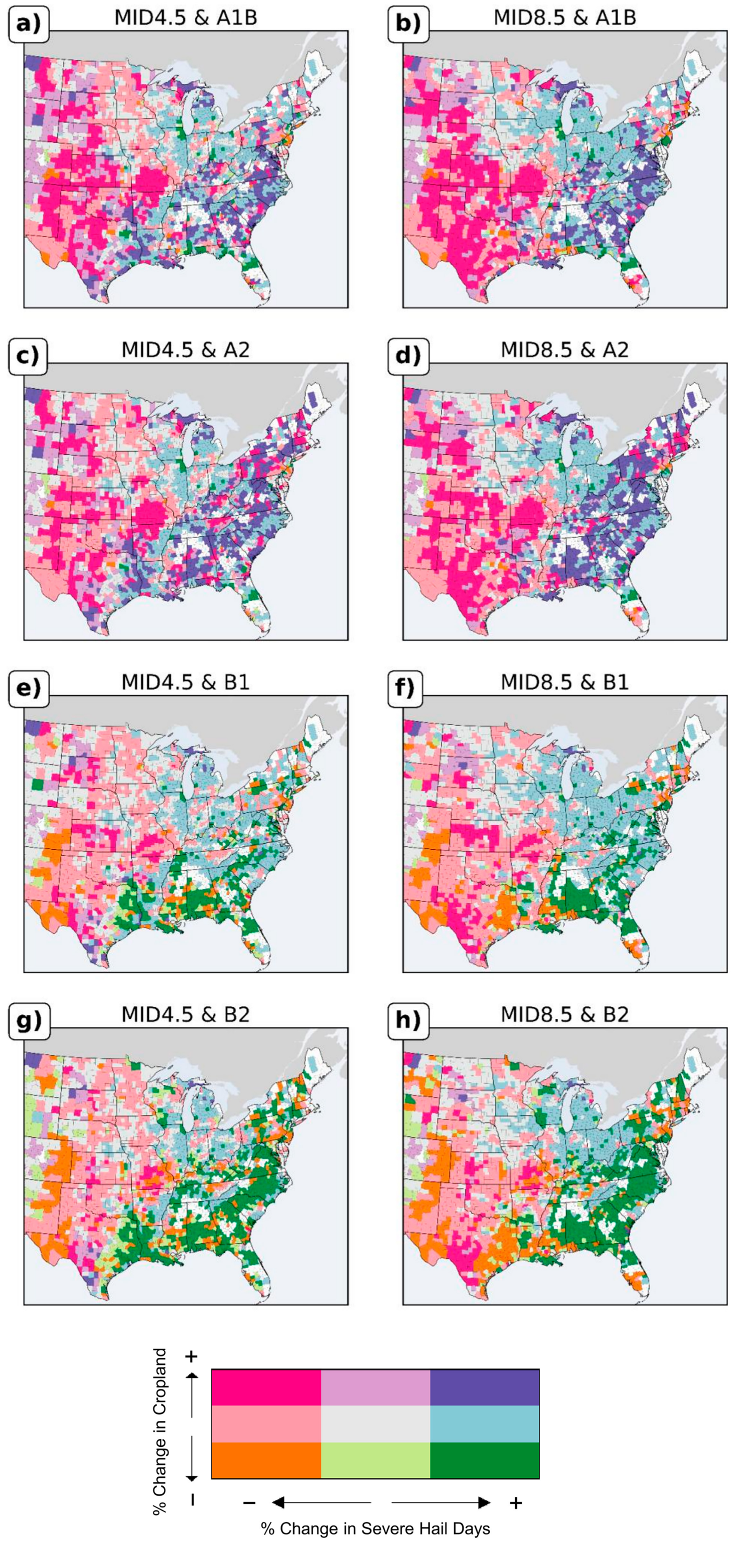

FIG. 9. Bivariate county-level changes in severe hail days paired with cropland coverage for midcentury WRF-BCC climate simulations and 2055 IPCC SRES cropland scenarios: (a) MID4.5 and A1B, (b) MID8.5 and A1B, (c) MID4.5 and A2, (d) MID8.5 and A2, (e) MID4.5 and B1, (f) MID8.5 and B1, (g) MID4.5 and B2, and (h) MID8.5 and B2. Colors represent the combined direction and magnitude of percent change in severe hail days and cropland coverage relative to historical conditions. Positive (negative) percent changes refer to severe hail-day or cropland changes > 20% (<−20%).

Authenticated lbundy@niu.edu | Downloaded 09/03/26 01:39 PM UTC

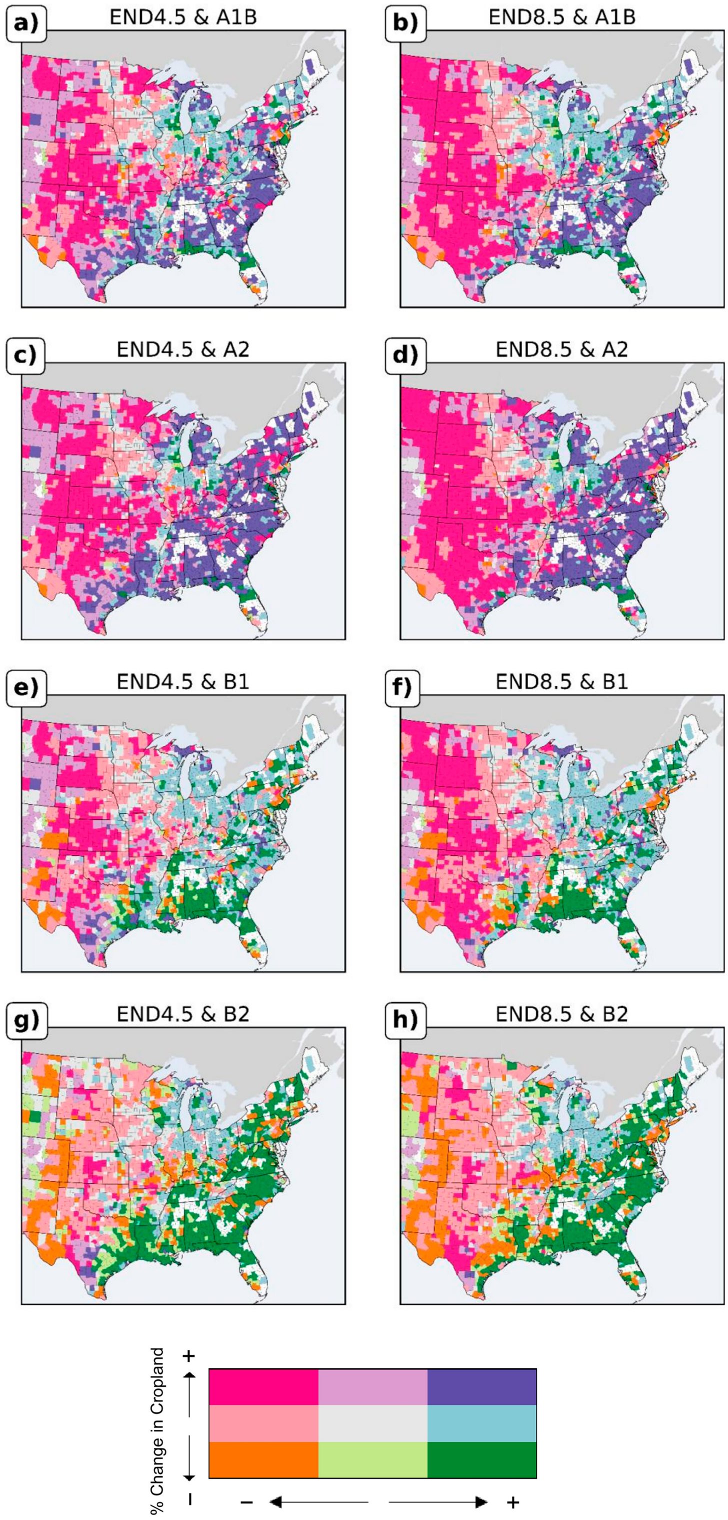

FIG. 10. As in Fig. 9, but for the end-of-century period.

Authenticated lbundy@niu.edu | Downloaded 09/03/26 01:39 PM UTC

4. Conclusions

Heightened crop demand has driven regional cropland expansion across the United States (Cassidy et al. 2013; Lark et al. 2015, 2020), coinciding with increasing weather- and climate-related losses (Changnon and Hewings 2001; Bouwer 2011). Such expansion introduces uncertainty not only for natural landscapes (Henwood 2010) but also for agricultural vulnerability to climate hazards (Steele and Hatfield 2018), particularly in regions with marginal biophysical capacity and frequent summer growing-season extremes (Lark et al. 2015, 2020). Disasters are fundamentally a product of hazard, exposure, and vulnerability (Ashley et al. 2014; IPCC 2014; Ashley and Strader 2016; Strader et al. 2018), and this study advances that framework by examining historical and projected crop-hail risk in the United States using a unique combination of cropland projections (Sohl et al. 2018a,b), severe hail climatologies (SPC 2024), crop-hail insurance data (RMA 2024), and high-resolution, convection-permitting climate simulations (Gensini et al. 2023).

Results underscore that the Midwest, with its sheer magnitude of cropland, faces the highest probability of hail impacting agricultural land each growing season. Yet, it is the Great Plains—where extensive cropland overlaps with the climatological maximum of severe hail—that emerges as the epicenter of historical and likely future crop-hail loss if projections hold true. This outcome reflects the "expanding bull's-eye effect" (Ashley et al. 2014), here applied directly for the first time in an agricultural context: disaster potential, or major crop yield loss, is defined less by total cropland acreage than by its spatial distribution relative to the hazard. Even with projected decreases in severe hail days, the expansion of cropland between the historical baseline and future periods across the Great Plains magnifies the likelihood that hail swaths will intersect farmland, sustaining, or even increasing future loss potential. Conversely, modest cropland changes in the Midwest and South paired with a projected increase in severe hail days also suggest heightened risk in regions not traditionally considered hail "hotspots."

From a management perspective, these findings highlight the need for proactive adaptation strategies, providing operational insights that could inform county-level risk rating adjustments or guide conservation incentives in high-risk areas. Additionally, these methods provide a foundation for future work, despite data limitations. Expanding to crop-specific datasets, phenological models, or other perils (e.g., drought, flooding, heat) would allow for richer assessments of how climate variability and land-cover change intersect to shape agricultural risk. Importantly, the framework demonstrated here can be extended internationally, informing global food-security analyses in regions where cropland expansion into marginal lands is accelerating. In sum, this study provides one of the first comprehensive frameworks for linking cropland changes and severe convective hazard projections, offering a novel basis for understanding and managing future crop-hail risk. For society at large, the persistence of hail risk despite projected climatological declines emphasizes the challenge of safeguarding food systems under climate change. Ensuring that crop production remains resilient to hail and other extreme weather hazards is not only an agricultural priority but also a cornerstone of food security in a period of increasing demand and volatility.

Acknowledgments. This research was supported by the National Science Foundation Awards 1637225 and 1800582 and National Oceanic and Atmospheric Administration Award NA22OAR4690645. The authors acknowledge high-performance computing support from Cheyenne (https://doi.org/10.5065/D6RX99HX) provided by NCAR's Computational and Information Systems Laboratory, sponsored by the National Science Foundation. MID simulations were performed on the Comet supercomputer, which is hosted by the San Diego Supercomputer Center at the University of California, San Diego. This computational resource was made available by the Atmospheric River Program (phases 2 and 3), which is supported by the California Department of Water Resources (Awards 4600013361 and 4600014294, respectively) and the U.S. Army Corps of Engineers Engineer Research and Development Center (Award USACE W912HZ-15-2-0019). We also acknowledge and thank Dr. Michael Papka (ANL) for data storage. This research used resources of the Argonne Leadership Computing Facility, which is a DOE Office of Science User Facility supported under Contract DE-AC02-06CH11357.

Data availability statement. All datasets used, except for the WRF-BCC and HailMC output, are publicly available.

REFERENCES

Abram, N., and Coauthors, 2019: Framing and context of the report supplementary material. *IPCC Special Report on the Ocean and Cryosphere in a Changing Climate*, H.-O. Pörtner et al., Eds., Cambridge University Press, 73–129, https://www.ipcc.ch/site/assets/uploads/sites/3/2019/11/SROCC_Ch01-SM_FINAL.pdf.

Allen, J. T., and M. K. Tippett, 2015: The characteristics of United States hail reports: 1955–2014. *Electron. J. Severe Storms Meteor.*, **10** (3), https://ejssm.com/ojs/index.php/site/article/view/60.

——, ——, and A. H. Sobel, 2015: An empirical model relating U.S. monthly hail occurrence to large-scale meteorological environment. *J. Adv. Model. Earth Syst.*, **7**, 226–243, https://doi.org/10.1002/2014MS000397.

Ashley, W. S., and S. M. Strader, 2016: Recipe for disaster: How the dynamic ingredients of risk and exposure are changing the tornado disaster landscape. *Bull. Amer. Meteor. Soc.*, **97**, 767–786, https://doi.org/10.1175/BAMS-D-15-00150.1.

——, S. Strader, T. Rosencrants, and A. J. Krmenec, 2014: Spatiotemporal changes in tornado hazard exposure: The case of the expanding bull's-eye effect in Chicago, Illinois. *Wea. Climate Soc.*, **6**, 175–193, https://doi.org/10.1175/WCAS-D-13-00047.1.

——, A. M. Haberlie, and V. A. Gensini, 2023: The future of supercells in the United States. *Bull. Amer. Meteor. Soc.*, **104**, E1–E21, https://doi.org/10.1175/BAMS-D-22-0027.1.

Barthel, F., and E. Neumayer, 2012: A trend analysis of normalized insured damage from natural disasters. *Climatic Change*, **113**, 215–237, https://doi.org/10.1007/s10584-011-0331-2.

Battaglia, M., C. Lee, W. Thomason, J. Fike, and A. Sadeghpour, 2019: Hail damage impacts on corn productivity: A review.

Authenticated lbundy@niu.edu | Downloaded 09/03/26 01:39 PM UTC

Crop Sci., **59** (1), 1–14, https://doi.org/10.2135/cropsci2018.04.0285.

Bendorf, J., and T. Schillerberg, 2024: Hail in the Midwest & impacts to agriculture. U.S. Department of Agriculture Rep., 3 pp., https://cropwatch.unl.edu/sites/unl.edu.ianr.extension.cropwatch/files/media/file/Midwest-Climate-Hub-hail-factsheet-2024.pdf.

Bolster, C. H., and Coauthors, 2023: Agriculture, food systems, and rural communities. *Fifth National Climate Assessment*, A. R. Crimmins et al., Eds., U.S. Global Change Research Program, 11-1–11-39, https://doi.org/10.7930/NCA5.2023.CH11.

Bouwer, L. M., 2011: Have disaster losses increased due to anthropogenic climate change? *Bull. Amer. Meteor. Soc.*, **92**, 39–46, https://doi.org/10.1175/2010BAMS3092.1.

Brimelow, J. C., W. R. Burrows, and J. M. Hanesiak, 2017: The changing hail threat over North America in response to anthropogenic climate change. *Nat. Climate Change*, **7**, 516–522, https://doi.org/10.1038/nclimate3321.

Bundy, L. R., V. A. Gensini, and M. S. Russo, 2022: Insured corn losses in the United States from weather and climate perils. *J. Appl. Meteor. Climatol.*, **61**, 969–988, https://doi.org/10.1175/JAMC-D-21-0245.1.

——, ——, W. S. Ashley, A. M. Haberlie, and D. Changnon, 2024: United States crop conditions: 1986–2022. *Agron. J.*, **116**, 1397–1416, https://doi.org/10.1002/agj2.21558.

——, K. N. Kaminski, A. M. Haberlie, W. S. Ashley, and V. A. Gensini, 2026: Derecho impacts on United States crop condition ratings and yield. *Agric. For. Meteor.*, **376**, 110913, https://doi.org/10.1016/j.agrformet.2025.110913.

Cassidy, E. S., P. C. West, J. S. Gerber, and J. A. Foley, 2013: Redefining agricultural yields: From tonnes to people nourished per hectare. *Environ. Res. Lett.*, **8**, 034015, https://doi.org/10.1088/1748-9326/8/3/034015.

Cecil, D. J., and C. B. Blankenship, 2012: Toward a global climatology of severe hailstorms as estimated by satellite passive microwave imagers. *J. Climate*, **25**, 687–703, https://doi.org/10.1175/JCLI-D-11-00130.1.

Changnon, D., S. A. Changnon, and S. S. Changnon, 2001: A method for estimating crop losses from hail in uninsured periods and regions. *J. Appl. Meteor.*, **40**, 84–91, https://doi.org/10.1175/1520-0450(2001)040<0084:AMFECL>2.0.CO;2.

Changnon, S. A., 1972: Examples of economic losses, from hail in the United States. *J. Appl. Meteor.*, **11**, 1128–1137, https://doi.org/10.1175/1520-0450(1972)011<1128:EOELFH>2.0.CO;2.

——, 1999: Data and approaches for determining hail risk in the contiguous United States. *J. Appl. Meteor.*, **38**, 1730–1739, https://doi.org/10.1175/1520-0450(1999)038<1730:DAAFDH>2.0.CO;2.

——, and G. J. D. Hewings, 2001: Losses from weather extremes in the United States. *Nat. Hazards Rev.*, **2**, 113–123, https://doi.org/10.1061/(ASCE)1527-6988(2001)2:3(113).

——, D. Changnon, E. R. Fosse, D. C. Hoganson, R. J. Roth, and J. M. Totsch, 1997: Effects of recent weather extremes on the insurance industry: Major implications for the atmospheric sciences. *Bull. Amer. Meteor. Soc.*, **78**, 425–436, https://doi.org/10.1175/1520-0477(1997)078<0425:EORWEO>2.0.CO;2.

——, ——, and S. D. Hilberg, 2009: Hailstorms across the nation: An atlas about hail and its damages. Illinois State Water Survey ISWS Contract Rep. CR-2009-12, 101 pp., https://hdl.handle.net/2142/15156.

Chemeris, A., Y. Liu, and A. P. Ker, 2022: Insurance subsidies, climate change, and innovation: Implications for crop yield resiliency. *Food Policy*, **108**, 102232, https://doi.org/10.1016/j.foodpol.2022.102232.

Childs, S. J., R. S. Schumacher, and S. M. Strader, 2020: Projecting end-of-century human exposure from tornadoes and severe hailstorms in eastern Colorado: Meteorological and population perspectives. *Wea. Climate Soc.*, **12**, 575–595, https://doi.org/10.1175/WCAS-D-19-0153.1.

Cintineo, J. L., T. M. Smith, V. Lakshmanan, H. E. Brooks, and K. L. Ortega, 2012: An objective high-resolution hail climatology of the contiguous United States. *Wea. Forecasting*, **27**, 1235–1248, https://doi.org/10.1175/WAF-D-11-00151.1.

Climate Action Tracker, 2025: USA. Accessed 6 May 2026, https://climateactiontracker.org/countries/usa/.

Coble, K. H., and B. J. Barnett, 2013: Why do we subsidize crop insurance? *Amer. J. Agric. Econ.*, **95**, 498–504, https://doi.org/10.1093/ajae/aas093.

Farm Service Agency, 2025: Conservation Reserve Program (CRP). USDA, accessed 15 October 2025, https://www.fsa.usda.gov/resources/programs/conservation-reserve-program.

Flanagan, P. X., R. Mahmood, T. Sohl, M. Svoboda, B. Wardlow, M. Hayes, and E. Rappin, 2021: Simulated atmospheric response to four projected land-use land-cover change scenarios for 2050 in the north-central United States. *Earth Interact.*, **25**, 177–194, https://doi.org/10.1175/EI-D-20-0019.1.

Freeman, A. C., and W. S. Ashley, 2017: Changes in the US hurricane disaster landscape: The relationship between risk and exposure. *Nat. Hazards*, **88**, 659–682, https://doi.org/10.1007/s11069-017-2885-4.

Gaines, M. D., M. G. Tulbure, V. Perin, R. Composto, and V. Tiwari, 2024: Projecting surface water area under different climate and development scenarios. *Earth's Future*, **12**, e2024EF004625, https://doi.org/10.1029/2024EF004625.

Gensini, V. A., and T. L. Mote, 2014: Estimations of hazardous convective weather in the United States using dynamical downscaling. *J. Climate*, **27**, 6581–6589, https://doi.org/10.1175/JCLI-D-13-00777.1.

——, and ——, 2015: Downscaled estimates of late 21st century severe weather from CCSM3. *Climatic Change*, **129**, 307–321, https://doi.org/10.1007/s10584-014-1320-z.

——, A. M. Haberlie, and P. T. Marsh, 2020: Practically perfect hindcasts of severe convective storms. *Bull. Amer. Meteor. Soc.*, **101**, E1259–E1278, https://doi.org/10.1175/BAMS-D-19-0321.1.

——, ——, and W. S. Ashley, 2023: Convection-permitting simulations of historical and possible future climate over the contiguous United States. *Climate Dyn.*, **60**, 109–126, https://doi.org/10.1007/s00382-022-06306-0.

——, W. S. Ashley, A. C. Michaelis, A. M. Haberlie, J. Goodin, and B. C. Wallace, 2024: Hailstone size dichotomy in a warming climate. *npj Climate Atmos. Sci.*, **7**, 185, https://doi.org/10.1038/s41612-024-00728-9.

Goldberg, Z. A., 2023: Solar energy development on farmland: Three prevalent perspectives of conflict, synergy and compromise in the United States. *Energy Res. Soc. Sci.*, **101**, 103145, https://doi.org/10.1016/j.erss.2023.103145.

Haberlie, A. M., W. S. Ashley, C. M. Battisto, and V. A. Gensini, 2022: Thunderstorm activity under intermediate and extreme climate change scenarios. *Geophys. Res. Lett.*, **49**, e2022GL098779, https://doi.org/10.1029/2022GL098779.

——, B. Wallace, W. S. Ashley, V. A. Gensini, and A. C. Michaelis, 2024: Mesoscale convective system activity in the United States under intermediate and extreme climate change scenarios. *Climatic Change*, **177**, 94, https://doi.org/10.1007/s10584-024-03752-z.

Authenticated lbundy@niu.edu | Downloaded 09/03/26 01:39 PM UTC

Harrison-Atlas, D., A. Lopez, and E. Lantz, 2022: Dynamic land use implications of rapidly expanding and evolving wind power deployment. *Environ. Res. Lett.*, **17**, 044064, https://doi.org/10.1088/1748-9326/ac5f2c.

Hausfather, Z., and G. P. Peters, 2020: Emissions—The 'business as usual' story is misleading. *Nature*, **577**, 618–620, https://doi.org/10.1038/d41586-020-00177-3.

Henwood, W. D., 2010: Toward a strategy for the conservation and protection of the world's temperate grasslands. *Great Plains Res.*, **20**, 121–134.

Hoogewind, K. A., M. E. Baldwin, and R. J. Trapp, 2017: The impact of climate change on hazardous convective weather in the United States: Insight from high-resolution dynamical downscaling. *J. Climate*, **30**, 10 081–10 100, https://doi.org/10.1175/JCLI-D-16-0885.1.

IPCC, 2014: *Climate Change 2014: Impacts, Adaptation and Vulnerability: Part A: Global and Sectoral Aspects.* C. B. Field et al., Eds., Cambridge University Press, 1140 pp.

Jain, A. N., L. Harris, N. Moyer, C. Brock, P. R. Roehrdanz, and A. Larsen, 2025: Assessing future environmental benefits of agricultural abandonment and recultivation. *Environ. Res. Lett.*, **20**, 074035, https://doi.org/10.1088/1748-9326/add9b0.

Janković, V., and D. M. Schultz, 2017: Atmosfear: Communicating the effects of climate change on extreme weather. *Wea. Climate Soc.*, **9**, 27–37, https://doi.org/10.1175/WCAS-D-16-0030.1.

Johnson, J. A., C. F. Runge, B. Senauer, J. Foley, and S. Polasky, 2014: Global agriculture and carbon trade-offs. *Proc. Natl. Acad. Sci. USA*, **111**, 12 342–12 347, https://doi.org/10.1073/pnas.1412835111.

Jones, B., and B. C. O'Neill, 2016: Spatially explicit global population scenarios consistent with the Shared Socioeconomic Pathways. *Environ. Res. Lett.*, **11**, 084003, https://doi.org/10.1088/1748-9326/11/8/084003.

Kaminski, K., W. S. Ashley, A. M. Haberlie, and V. A. Gensini, 2025: Future derecho potential in the United States. *J. Climate*, **38**, 3–26, https://doi.org/10.1175/JCLI-D-23-0633.1.

Katz, R. W., and R. R. Garcia, 1981: Statistical relationships between hailfall and damage to wheat. *Agric. Meteor.*, **24**, 29–43, https://doi.org/10.1016/0002-1571(81)90031-5.

Kendon, E. J., A. F. Prein, C. A. Senior, and A. Stirling, 2021: Challenges and outlook for convection-permitting climate modelling. *Philos. Trans. Roy. Soc.*, **A379**, 20190547, https://doi.org/10.1098/rsta.2019.0547.

Klein, R. N., and C. A. Shapiro, 2011: Evaluating hail damage to corn. Board of Regents of the University of Nebraska, University Nebraska–Lincoln Extension Rep., 8 pp.

Kloster, S., N. M. Mahowald, J. T. Randerson, and P. J. Lawrence, 2012: The impacts of climate, land use, and demography on fires during the 21st century simulated by CLM-CN. *Biogeosciences*, **9**, 509–525, https://doi.org/10.5194/bg-9-509-2012.

Lark, T. J., J. M. Salmon, and H. K. Gibbs, 2015: Cropland expansion outpaces agricultural and biofuel policies in the United States. *Environ. Res. Lett.*, **10**, 044003, https://doi.org/10.1088/1748-9326/10/4/044003.

——, B. Larson, I. Schelly, S. Batish, and H. K. Gibbs, 2019: Accelerated conversion of native prairie to cropland in Minnesota. *Environ. Conserv.*, **46**, 155–162, https://doi.org/10.1017/S0376892918000437.

——, S. A. Spawn, M. Bougie, and H. K. Gibbs, 2020: Cropland expansion in the United States produces marginal yields at high costs to wildlife. *Nat. Commun.*, **11**, 4295, https://doi.org/10.1038/s41467-020-18045-z.

Li, Y., K. Guan, G. D. Schnitkey, E. DeLucia, and B. Peng, 2019: Excessive rainfall leads to maize yield loss of a comparable magnitude to extreme drought in the United States. *Global Change Biol.*, **25**, 2325–2337, https://doi.org/10.1111/gcb.14628.

Lindsey, A. J., and Coauthors, 2024: Severe storm damage and short-term weather stresses on corn: A review. *Crop Sci.*, **64**, 1129–1166, https://doi.org/10.1002/csc2.21212.

Lisboa, I. P., and Coauthors, 2024: Evaluating the yield of surviving plants from early-season hail damage in corn: A field survey. *Agrosyst. Geosci. Environ.*, **7**, e20533, https://doi.org/10.1002/agg2.20533.

Liu, C., and Coauthors, 2017: Continental-scale convection-permitting modeling of the current and future climate of North America. *Climate Dyn.*, **49**, 71–95, https://doi.org/10.1007/s00382-016-3327-9.

Lobell, D. B., M. J. Roberts, W. Schlenker, N. Braun, B. B. Little, R. M. Rejesus, and G. L. Hammer, 2014: Greater sensitivity to drought accompanies maize yield increase in the U.S. midwest. *Science*, **344**, 516–519, https://doi.org/10.1126/science.1251423.

MacMillan, K. P., 2023: Hail damage research report. Soybean and Pulse Agronomy Lab Rep., 18 pp., https://www.manitobapulse.ca/wp-content/uploads/2023/07/Hail-Damage-Research-Reports.pdf.

Mai, T., A. Lopez, M. Mowers, and E. Lantz, 2021: Interactions of wind energy project siting, wind resource potential, and the evolution of the U.S. power system. *Energy*, **223**, 119998, https://doi.org/10.1016/j.energy.2021.119998.

Meinshausen, M., and Coauthors, 2020: The shared socio-economic pathway (SSP) greenhouse gas concentrations and their extensions to 2500. *Geosci. Model Dev.*, **13**, 3571–3605, https://doi.org/10.5194/gmd-13-3571-2020.

Montefiore, L. R., N. G. Nelson, M. D. Staudinger, and A. Terando, 2023: Vulnerability of estuarine systems in the contiguous United States to water quality change under future climate and land-use. *Earth's Future*, **11**, e2022EF002884, https://doi.org/10.1029/2022EF002884.

Moss, R. H., and Coauthors, 2010: The next generation of scenarios for climate change research and assessment. *Nature*, **463**, 747–756, https://doi.org/10.1038/nature08823.

Murillo, E. M., C. R. Homeyer, and J. T. Allen, 2021: A 23-year severe hail climatology using GridRad MESH observations. *Mon. Wea. Rev.*, **149**, 945–958, https://doi.org/10.1175/mwr-d-20-0178.1.

Nakicenovic, N., and Coauthors, 2000: IPCC special report on emissions scenarios. IPCC Rep., 28 pp., https://escholarship.org/uc/item/9sz5p22f.

NASS, 2024: Quick stats tools. U.S. Department of Agriculture, accessed 3 November 2024, https://www.nass.usda.gov/Quick_Stats/.

NWS, 2025: The 3-tiered approach to keeping you alerted to severe weather. Accessed 1 October 2025, https://www.weather.gov/jkl/severeproducts.

Obolensky, M., 2025: Protect or prepare? Crop insurance and adaptation in a changing climate. Job Market Paper, 75 pp., https://www.parisschoolofeconomics.eu/app/uploads/2025/01/obolensky_crop_insurance_JMP-programme.pdf.

Perry, E. D., J. Yu, and J. Tack, 2020: Using insurance data to quantify the multidimensional impacts of warming temperatures on yield risk. *Nat. Commun.*, **11**, 4542, https://doi.org/10.1038/s41467-020-17707-2.

Pielke, R. A., Jr., 2005: Attribution of disaster losses. *Science*, **310**, 1615–1616, https://doi.org/10.1126/science.310.5754.1615c.

Authenticated lbundy@niu.edu | Downloaded 09/03/26 01:39 PM UTC

——, J. Gratz, C. W. Landsea, D. Collins, M. A. Saunders, and R. Musulin, 2008: Normalized hurricane damage in the United States: 1900–2005. *Nat. Hazards Rev.*, **9**, 29–42, https://doi.org/10.1061/(ASCE)1527-6988(2008)9:1(29).

Prein, A. F., C. Liu, K. Ikeda, S. B. Trier, R. M. Rasmussen, G. J. Holland, and M. P. Clark, 2017: Increased rainfall volume from future convective storms in the US. *Nat. Climate Change*, **7**, 880–884, https://doi.org/10.1038/s41558-017-0007-7.

Ramankutty, N., and J. A. Foley, 1999a: Estimating historical changes in global land cover: Croplands from 1700 to 1992. *Global Biogeochem. Cycles*, **13**, 997–1027, https://doi.org/10.1029/1999GB900046.

——, and ——, 1999b: Estimating historical changes in land cover: North American croplands from 1850 to 1992. *Global Ecol. Biogeogr.*, **8**, 381–396, https://doi.org/10.1046/j.1365-2699.1999.00141.x.

Rasmussen, K. L., A. F. Prein, R. M. Rasmussen, K. Ikeda, and C. Liu, 2020: Changes in the convective population and thermodynamic environments in convection-permitting regional climate simulations over the United States. *Climate Dyn.*, **55**, 383–408, https://doi.org/10.1007/s00382-017-4000-7.

Raupach, T. H., and Coauthors, 2021: The effects of climate change on hailstorms. *Nat. Rev. Earth Environ.*, **2**, 213–226, https://doi.org/10.1038/s43017-020-00133-9.

Renard, D., and D. Tilman, 2019: National food production stabilized by crop diversity. *Nature*, **571**, 257–260, https://doi.org/10.1038/s41586-019-1316-y.

Reyes, J., and E. Elias, 2019: Spatio-temporal variation of crop loss in the United States from 2001 to 2016. *Environ. Res. Lett.*, **14**, 074017, https://doi.org/10.1088/1748-9326/ab1ac9.

——, ——, E. Haacker, A. Kremen, L. Parker, and C. Rottler, 2020: Assessing agricultural risk management using historic crop insurance loss data over the Ogallala Aquifer. *Agric. Water Manage.*, **232**, 106000, https://doi.org/10.1016/j.agwat.2020.106000.

Riahi, K., and Coauthors, 2011: RCP 8.5—A scenario of comparatively high greenhouse gas emissions. *Climatic Change*, **109**, 33–57, https://doi.org/10.1007/s10584-011-0149-y.

——, and Coauthors, 2017: The Shared Socioeconomic Pathways and their energy, land use, and greenhouse gas emissions implications: An overview. *Global Environ. Change*, **42**, 153–168, https://doi.org/10.1016/j.gloenvcha.2016.05.009.

RMA, 2024: Cause of loss information—Summary of business data. U.S. Department of Agriculture Risk Management Agency, accessed 15 March 2024, https://www.rma.usda.gov/tools-reports/summary-of-business/cause-of-loss.

——, 2025: AgRisk viewer. USDA Southwest Climate Hub, accessed 4 October 2025, https://agrisk.jornada.nmsu.edu/rma/rma-data-viewer.html.

Robinson, E. D., R. J. Trapp, and M. E. Baldwin, 2013: The geospatial and temporal distributions of severe thunderstorms from high-resolution dynamical downscaling. *J. Appl. Meteor. Climatol.*, **52**, 2147–2161, https://doi.org/10.1175/JAMC-D-12-0131.1.

Rosencrants, T. D., and W. S. Ashley, 2015: Spatiotemporal analysis of tornado exposure in five US metropolitan areas. *Nat. Hazards*, **78**, 121–140, https://doi.org/10.1007/s11069-015-1704-z.

Schwalm, C. R., S. Glendon, and P. B. Duffy, 2020: RCP8.5 tracks cumulative CO_2 emissions. *Proc. Natl. Acad. Sci. USA*, **117**, 19656–19657, https://doi.org/10.1073/pnas.2007117117.

Simmons, K. M., D. Sutter, and R. Pielke, 2013: Normalized tornado damage in the United States: 1950–2011. *Environ. Hazards*, **12**, 132–147, https://doi.org/10.1080/17477891.2012.738642.

Sohl, T. L., K. L. Sayler, M. A. Drummond, and T. R. Loveland, 2007: The FORE-SCE model: A practical approach for projecting land cover change using scenario-based modeling. *J. Land Use Sci.*, **2**, 103–126, https://doi.org/10.1080/17474230701218202.

——, and Coauthors, 2012: Spatially explicit land-use and land-cover scenarios for the Great Plains of the United States. *Agric. Ecosyst. Environ.*, **153**, 1–15, https://doi.org/10.1016/j.agee.2012.02.019.

——, and Coauthors, 2014: Spatially explicit modeling of 1992–2100 land cover and forest stand age for the conterminous United States. *Ecol. Appl.*, **24**, 1015–1036, https://doi.org/10.1890/13-1245.1.

——, R. Reker, M. Bouchard, K. Sayler, J. Dornbierer, S. Wika, R. Quenzer, and A. Friesz, 2018a: Modeled historical land use and land cover for the conterminous United States: 1938–1992. U.S. Geological Survey, accessed 10 March 2024, https://doi.org/10.5066/F7KK99RR.

——, and Coauthors, 2018b: Conterminous United States land cover projections—1992 to 2100. U.S. Geological Survey, accessed 10 March 2024, https://doi.org/10.5066/P95AK9HP.

——, J. Dornbierer, S. Wika, and C. Robison, 2019: Remote sensing as the foundation for high-resolution United States landscape projections—The Land Change Monitoring, Assessment, and Projection (LCMAP) initiative. *Environ. Modell. Software*, **120**, 104495, https://doi.org/10.1016/j.envsoft.2019.104495.

SPC, 2024: SVRGIS. NWS, Storm Prediction Center, accessed 10 March 2024, https://www.spc.noaa.gov/gis/svrgis/.

Steele, R., and J. L. Hatfield, 2018: Navigating climate-related challenges on working lands: A special issue by the USDA Climate Hubs and their partners. *Climatic Change*, **146** (1–2), 1–3, https://doi.org/10.1007/s10584-017-2129-3.

Stinnett, S. N., V. A. Gensini, A. M. Haberlie, A. C. Michaelis, and W. S. Ashley, 2024: Changes in extreme daily precipitation over the contiguous United States from convection-permitting simulations. *J. Appl. Meteor. Climatol.*, **63**, 1523–1543, https://doi.org/10.1175/JAMC-D-23-0206.1.

Strader, S. M., 2018: Spatiotemporal changes in conterminous US wildfire exposure from 1940 to 2010. *Nat. Hazards*, **92**, 543–565, https://doi.org/10.1007/s11069-018-3217-z.

——, W. S. Ashley, A. Irizarry, and S. Hall, 2015a: A climatology of tornado intensity assessments. *Meteor. Appl.*, **22**, 513–524, https://doi.org/10.1002/met.1482.

——, W. Ashley, and J. Walker, 2015b: Changes in volcanic hazard exposure in the Northwest USA from 1940 to 2100. *Nat. Hazards*, **77**, 1365–1392, https://doi.org/10.1007/s11069-015-1658-1.

——, T. J. Pingel, and W. S. Ashley, 2016: A Monte Carlo model for estimating tornado impacts. *Meteor. Appl.*, **23**, 269–281, https://doi.org/10.1002/met.1552.

——, W. S. Ashley, T. J. Pingel, and A. J. Krmenec, 2017a: Observed and projected changes in United States tornado exposure. *Wea. Climate Soc.*, **9**, 109–123, https://doi.org/10.1175/WCAS-D-16-0041.1.

——, ——, ——, and ——, 2017b: Projected 21st century changes in tornado exposure, risk, and disaster potential. *Climatic Change*, **141**, 301–313, https://doi.org/10.1007/s10584-017-1905-4.

——, ——, ——, and ——, 2018: How land use alters the tornado disaster landscape. *Appl. Geogr.*, **94**, 18–29, https://doi.org/10.1016/j.apgeog.2018.03.005.

Authenticated lbundy@niu.edu | Downloaded 09/03/26 01:39 PM UTC

——, V. A. Gensini, W. S. Ashley, and A. N. Wagner, 2024: Changes in tornado risk and societal vulnerability leading to greater tornado impact potential. *npj Nat. Hazards*, **1**, 20, https://doi.org/10.1038/s44304-024-00019-6.

Tang, B. H., V. A. Gensini, and C. R. Homeyer, 2019: Trends in United States large hail environments and observations. *npj Climate. Atmos. Sci.*, **2**, 45, https://doi.org/10.1038/s41612-019-0103-7.

Tebaldi, C., and Coauthors, 2021: Climate model projections from the Scenario Model Intercomparison Project (ScenarioMIP) of CMIP6. *Earth Syst. Dyn.*, **12**, 253–293, https://doi.org/10.5194/esd-12-253-2021.

Thompson, G., P. R. Field, R. M. Rasmussen, and W. D. Hall, 2008: Explicit forecasts of winter precipitation using an improved bulk microphysics scheme. Part II: Implementation of a new snow parameterization. *Mon. Wea. Rev.*, **136**, 5095–5115, https://doi.org/10.1175/2008MWR2387.1.

Thomson, A. M., and Coauthors, 2011: RCP4.5: A pathway for stabilization of radiative forcing by 2100. *Climatic Change*, **109**, 77, https://doi.org/10.1007/s10584-011-0151-4.

Trapp, R. J., and K. A. Hoogewind, 2016: The realization of extreme tornadic storm events under future anthropogenic climate change. *J. Climate*, **29**, 5251–5265, https://doi.org/10.1175/JCLI-D-15-0623.1.

——, E. D. Robinson, M. E. Baldwin, N. S. Diffenbaugh, and B. R. J. Schwedler, 2011: Regional climate of hazardous convective weather through high-resolution dynamical downscaling. *Climate Dyn.*, **37**, 677–688, https://doi.org/10.1007/s00382-010-0826-y.

——, K. A. Hoogewind, and S. Lasher-Trapp, 2019: Future changes in hail occurrence in the United States determined through convection-permitting dynamical downscaling. *J. Climate*, **32**, 5493–5509, https://doi.org/10.1175/JCLI-D-18-0740.1.

van Vuuren, D. P., and T. R. Carter, 2014: Climate and socioeconomic scenarios for climate change research and assessment: Reconciling the new with the old. *Climatic Change*, **122**, 415–429, https://doi.org/10.1007/s10584-013-0974-2.

Vorst, J. V., 1993: Assessing hail damage to corn. National Corn Handbook Project, Purdue University Cooperative Extension Service, https://www.extension.purdue.edu/extmedia/nch/nch-1.html.

Wallace, B., A. M. Haberlie, V. A. Gensini, W. S. Ashley, and A. C. Michaelis, 2025: Cause and characteristics of changes in mesoscale convective systems within a convection-permitting regional climate model. *J. Climate*, **38**, 461–479, https://doi.org/10.1175/JCLI-D-24-0251.1.

Weisman, M. L., W. C. Skamarock, and J. B. Klemp, 1997: The resolution dependence of explicitly modeled convective systems. *Mon. Wea. Rev.*, **125**, 527–548, https://doi.org/10.1175/1520-0493(1997)125<0527:TRDOEM>2.0.CO;2.

West, P. C., H. K. Gibbs, C. Monfreda, J. Wagner, C. C. Barford, S. R. Carpenter, and J. A. Foley, 2010: Trading carbon for food: Global comparison of carbon stocks vs. crop yields on agricultural land. *Proc. Natl. Acad. Sci. USA*, **107**, 19 645–19 648, https://doi.org/10.1073/pnas.1011078107.

Wimberly, M. C., L. L. Janssen, D. A. Hennessy, M. Luri, N. M. Chowdhury, and H. Feng, 2017: Cropland expansion and grassland loss in the eastern Dakotas: New insights from a farm-level survey. *Land Use Policy*, **63**, 160–173, https://doi.org/10.1016/j.landusepol.2017.01.026.

Young, C. E., M. L. Vandeveer, and R. D. Schnepf, 2001: Production and price impacts of U.S. crop insurance programs. *Amer. J. Agric. Econ.*, **83**, 1196–1203, https://doi.org/10.1111/0002-9092.00267.

Yu, Z., and C. Lu, 2018: Historical cropland expansion and abandonment in the continental U.S. during 1850 to 2016. *Global Ecol. Biogeogr.*, **27**, 322–333, https://doi.org/10.1111/geb.12697.

Yue, Y., L. Zhou, A. X. Zhu, and X. Ye, 2019: Vulnerability of cotton subjected to hail damage. *PLOS ONE*, **14**, e0210787, https://doi.org/10.1371/journal.pone.0210787.

Zeeb, A. W., W. S. Ashley, A. M. Haberlie, V. A. Gensini, and A. C. Michaelis, 2024: Supercell precipitation contribution to the United States hydroclimate. *Int. J. Climatol.*, **44**, 1489–1512, https://doi.org/10.1002/joc.8395.

Authenticated lbundy@niu.edu | Downloaded 09/03/26 01:39 PM UTC